Accepted Manuscript

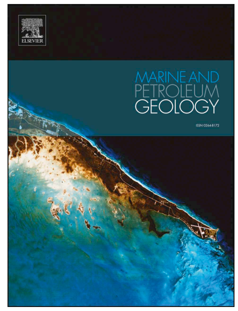

Origin and anatomy of two different types of mass-transport complexes: A 3D seismic case study from the northern South China Sea margin

Chenglin Gong, Yingmin Wang, David M. Hodgson, Weilin Zhu, Weiguo Li, Qiang Xu, Dong Li

PII: S0264-8172(14)00075-0

DOI: 10.1016/j.marpetgeo.2014.03.006

Reference: JMPG 1932

To appear in: *Marine and Petroleum Geology*

Received Date: 10 November 2013

Revised Date: 21 February 2014

Accepted Date: 9 March 2014

Origin and anatomy of two different types of mass-transport complexes: A 3D seismic case study from the northern South China Sea margin

Chenglin Gong[a, b *], Yingmin Wang[a, b *], David M. Hodgson[c], Weilin Zhu[d], Weiguo Li[e], Qiang Xu[f], Dong Li[f]

[a] State Key Laboratory of Petroleum Resources and Prospecting (China University of Petroleum, Beijing), Beijing 102249, People's Republic of China
[b] College of Geosciences, China University of Petroleum (Beijing), Beijing 102249, People's Republic of China
[c] Stratigraphy Group, School of Earth and Environment, University of Leeds, Leeds LS2 9JT, UK
[d] China National Offshore Oil Corporation Ltd (CNOOC)., Beijing 100010, People's Republic of China
[e] BP America Inc., Houston, TX, United States
[f] CNOOC Research Center, Beijing 100027, People's Republic of China

A B S T R A C T

Integration of 2D and 3D seismic data from the Qiongdongnan Basin along the northwestern South China Sea margin has enabled the seismic stratigraphy, seismic geomorphology and emplacement mechanisms of eight separate, previously undocumented, mass-transport complexes (MTCs) to be characterized. The MTCs can be grouped into two types:

(1) Localized detached MTCs, which are confined to submarine canyons and cover hundreds of km^2, consist of a few tens of km^3 remobilized sediments and show long striations at their base. They resulted from small-scale mass-wasting processes induced by regional tectonic events and and gravitational instabilities on canyon margins.

* Correspondence: Chenglin Gong, State Key Laboratory of Petroleum Resources and Prospecting (China University of Petroleum, Beijing), Fuxue Road No. 18, Changping, Beijing 102249, China. Weiguo Li, BP America Inc., Westlake Park Blvd., Houston, TX, United States 77079.
E-mail: chenglingong@hotmail.com (C. Gong), wgliuh@gmail.com (W. Li)

(2) Regional attached MTCs occur within semi-confined or unconfined settings and are distributed roughly perpendicular to the strike of the regional slope. Attached MTCs occupy hundreds to thousands of km^2 and are composed of tens to hundreds of km^3 of remobilized sediments. They contain headwall escarpments, translated blocks, remnant blocks, pressure ridges, and basal striations and cat-claw grooves. They were created by large-scale mass-wasting processes triggered by high sedimentation rates, slope oversteepening by shelf-edge deltas, and seismicity.

Our results show that MTCs may act as both lateral and top seals for underlying hydrocarbon reservoirs and could create MTC-related stratigraphic traps that represent potential drilling targets on continental margins, helping to identify MTC-related hydrocarbon traps.

Keywords: Mass-transport complexes, the northern South China Sea margin, seismic stratigraphy, seismic geomorphology, MTC-related hydrocarbon traps

1. Introduction

As petroleum exploration and production moves into greater water depths, and the availability of high-quality seismic data from continental margins becomes more widespread, mass-wasting processes and their deposits, MTCs, have been the focus of research (e.g. Canals et al., 2004; Weimer and Shipp, 2004; Evans et al., 2005; Moscardelli et al., 2006, 2012; Jackson, 2011, 2012; Shipp et al., 2011; Olafiranye et al., 2013). This is because they: (1) constitute a major component of the stratigraphy in many deep-water siliciclastic systems (Moscardelli et al., 2006; Posamentier and Walker 2008; Gong et al., 2011; Ogiesoba and Hammes, 2012; Olafiranye et al., 2013); (2) transport large volumes of sediments from continental shelves and/or upper slope into deep-water settings (Canals et al., 2004; Haflidason et al., 2005; Hjelstuen et al., 2007; Talling et al., 2007); (3) represent significant geohazards for coastal communities, nearshore navigation, and seabed infrastructure (Shipp et al., 2004; Weimer and Shipp, 2004; Mosher et al., 2010; Shipp and Lu, 2011; Zhu et al., 2011; Jackson, 2012); (4) need to be considered in the assessment of deep-water drilling programs (Moscardelli et al., 2006; Algar et al., 2011; Richardson et al., 2011; Shipp and Lu, 2011); and (5) can act as seals and poor reservoirs (Moscardelli et al., 2006; Weimer and Slatt, 2007; Riedel et al., 2012).

Generally, MTCs are considered to be poor reservoirs due to low porosities and permeabilities (e.g. Shipp et al., 2004; Moscardelli et al., 2006; Weimer and Slatt, 2007; Zhu et al., 2011), although sand-prone MTCs have been recognized (e.g., the eastern Mexico; Loucks et al., 2011). They can act as seals for underlying petroleum reservoirs, giving rise to alternative exploration targets in many parts of the world (Moscardelli et al., 2006; Weimer and Slatt, 2007; Zhu et al., 2011). However, the exploration significance of MTCs remains understudied.

Three-dimensional seismic data have proven to be one of the most powerful tools for the geological investigation of both ancient and recent MTCs (Moscardelli et al., 2006, 2012; Moscardelli and Wood, 2008; Jackson, 2011, 2012; Riedel et al., 2012; Olafiranye et al., 2013). A number of component elements of MTCs, such as basal grooves, remnant blocks, megaclasts, pressure ridges, have been recognized by many geologists from the analysis of 2D and/or 3D seismic data from deep-water basins worldwide (Moscardelli et al., 2006, 2012; Moscardelli and Wood, 2008; Bull et al., 2009; Jackson, 2011, 2012). However, there is scope for more quantitative approaches to the analysis of MTCs and their component elements using seismic data. Several aspects of MTCs, particularly their geomorphological characteristics, triggering mechanisms, and exploration significance, are still not fully understood (Canals et al., 2004; Weimer and Shipp, 2004; Evans et al., 2005; Shipp et al., 2011).

Despite continuing investigation of MTCs worldwide, studies of MTCs in the northern South China Sea margin are still limited. Zhu et al. (2011), however, documented the external morphology and internal architecture of several MTCs in Yinggehai Basin along the northwestern South China Sea margin (see Fig. 1 for their study area). MTCs constitute more than 60% of the Pliocene-Quaternary succession in the Qiongdongnan Basin (Gong et al., 2011). In contrast to the MTCs documented by Zhu et al. (2011) and many other studies, MTCs occurring in the study area of the

Qiongdongnan Basin are unusual because they are distributed both subparallel and roughly perpendicular to the strike of the regional slope. In addition, increased exploration activities in the study area and the northern South China Sea margin require characterization of these MTCs and understanding their roles in controlling hydrocarbon accumulations. The widespread occurrence of the best-developed MTCs and rich amount of data in the Qiongdongnan Basin permit (1) investigation of cross-sectional seismic expression and geomorphological characteristics of MTCs ; (2) discussion of possible triggering mechanisms of the studied MTCs; and (3) addressing MTC-related hydrocarbon trapping mechanisms. Our results will contribute to a better understanding of the origin and emplacement processes of MTCs and the prediction and identification of MTC-related hydrocarbon traps on continental margins.

2. Regional setting and the study area

The South China Sea is the largest (> 3.5×10^6 km^2) and deepest (> 5000 m) marginal sea along the western Pacific Ocean (Fig. 1). Several Cenozoic rift basins developed along the northern South China Sea margin, and from west to east they are the Beibuwan Basin, Yinggehai Basin, Qiongdongnan Basin, Pearl River Mouth Basin, and Taixinan Basin (Xie et al., 2006, 2008; Gong et al., 2013) (Fig. 1). The study area is located in the Qiongdongnan Basin, which is bounded to the west by the Red River Fault Zone and to the east by Pearl River Mouth Basin (Zhu et al., 2011; Gong et al., 2013) (Fig. 1).

The evolution of the Qiongdongnan Basin is closely linked to the strike-slip movements along the Red River Fault, which underwent sinistral slip during the period of 35～20 Ma and dextral movement since 5.5 Ma (Xie et al., 2006, 2008; Gong et al., 2011; Zhu et al., 2011). Driven by the strike-slip movement of the Red River Fault, Qiongdongnan Basin underwent two tectonic stages, namely a rifting stage from Paleocene to Early Oligocene, and a post-rifting stage from Early Miocene to Quaternary (Xie et al., 2006, 2008; Gong et al., 2011; Zhu et al., 2011). The fill of the Qiongdongnan Basin can be divided into syn-rift and post-rift supersequences, separated by a regionally important unconformity, the T60 surface, dated at 23.3 Ma (Zhu, et al., 2009; Gong et al., 2011). Neritic, deltaic and nearshore environments and the associated depositional systems are widely developed within the syn-rift supersequence (Xie et al., 2006, 2008). 'Typical' deep-water deposits (e.g., the Central submarine canyon, deep-marine channels, and MTCs, etc.) became widely developed within the post-rift supersequence, in response to the development of a prominent shelf-slope-basin physiography from 5.5 Ma onwards (Xie et al., 2006, 2008; Gong et al., 2011). The Central submarine canyon occurring in the study area is the largest deep-marine canyons in the northern South China Sea margin, has a total length of approximately 425 km, width of 3 to 12 km and an average area of 50,000 km^2 and show 'S' shape in plan view (Gong et al., 2011). Previously undocumented MTCs developed within the post-rift supersequence in the Qiongdongnan Basin are the focus of this study (Figs. 1 to 3).

3. Database and methodology

3.1 Database

The primary source of data used in this case is 1670 km^2 of 3D seismic data, tied to 2D regional seismic transects from the Qiongdongnan Basin (Fig. 1), which were acquired and provided by China National Offshore Oil Corporation (CNOOC). The dominant frequency of the time-migrated volume varies with depth, but is approximately 40 Hz for the interval of interest, with an estimated vertical resolution of ～15-20 m. The bin spacing of the time-migrated volume used in this study is 25 m × 12.5 m and has a 4 ms vertical sampling rate. The regional 2D seismic lines have a dominant frequency of ～30 Hz in the interval of interest, with an estimated vertical resolution of ～20-30 m. Both 2D and 3D seismic-reflection data were processed to zero phase and are displayed using 'SEG reverse polarity', where an increase in acoustic impedance is represented by a negative (trough) reflection event.

3.2 Methodology

Eight intervals of chaotic seismic facies (MTC1 to MTC8 from chronologically oldest to youngest), together with eight basal bounding surfaces (numbered from BS1 to BS8 from chronologically oldest to youngest), were identified in the Pliocene-Quaternary sedimentary interval in the Qiongdongnan Basin (Figs. 2 and 3). Three-dimensional perspective view maps of the eight basal bounding surfaces were generated (Figs. 4A to 11A), in order to understand bathymetric controls on the development of their overlying MTCs. Depth measurements were estimated, using 2000 m/s for the shallow siliciclastics in the study interval of interest and 1500 m/s for seawater.

This study is principally based on 'classical' 2D seismic facies analysis (Vail et al., 1977) and 3D seismic geomorphology approach (Posamentier et al., 2007), through which the stratigraphic architecture and seismic geomorphology of the documented MTCs and their component elements are quantitatively analyzed. Two-way traveltime (TWT) structural maps of the basal bounding surfaces of the studied MTCs were made in order to understand the topographic controls on the development of their overlying MTCs. Coherence images provide enhanced visualization of small-scale depositional features and allow accurate mapping the external morphology and internal architecture of the documented MTCs. Root-mean-square (RMS) amplitude is a seismic attribute that calculates the square root of the sum of time-domain energy (square of amplitude), affording high amplitudes the maximum opportunity to stand out from background contamination. RMS amplitude, therefore, can be used to describe the internal architecture of the documented seismic facies. 3D coherence probes, amplitude cubes and RMS attribute probes were created and are used to delineate the plan-view morphology of the documented MTCs and their component elements, using Landmark Seisworks, PostStack/PAL, and GeoProbe software.

4. 3D seismic stratigraphy and geomorphology of the documented MTCs and their component elements

Ten seismic facies were recognized in the documented MTCs in the Qiongdongnan Basin study area based on seismic reflection configuration (reflection continuity and amplitude), cross-sectional geometry and stratal terminations. Interpretations of seismic facies are based on recognition criteria established from published seismic-reflection datasets (e.g. Posamentier and Kolla, 2003; Shipp et al., 2004; Moscardelli et al., 2006, 2012; Bull et al., 2009; Gamboa et al. 2010; Jackson, 2011, 2012; Olafiranye et al., 2013). See Table 1 for a complete description and interpretation of all seismic facies.

4.1 Seismic facies description

4.1.1 Seismic facies 1: Irregular-shaped chaotic seismic facies

Seismic facies 1 is made up of chaotic, low-amplitude reflections with variable seismic reflection continuity and displays irregular-shaped cross-sectional geometry (cool color-shaded areas in Fig. 4C; Table 1). Reflections associated with this seismic facies are inclined towards canyon margins and downlap toward the thalweg of submarine canyons (Fig. 4C; Table 1). In plan form, this seismic facies exhibits an irregular morphology and can cover an area ranging from tens to hundreds of square kilometers (Fig. 4B; Table 1). In seismic geomorphic images, it is represented by light-colored zones and occurs on both flanks of the Central submarine canyon (Fig. 4B and 5B; Table 1).

4.1.2 Seismic facies 2: Long linear seismic facies

Seismic facies 2 is represented by laterally discontinuous, alternating high- and low-amplitude reflections (Fig. 5C; Table 1). This seismic facies is expressed in map view as light-colored, narrow, west-east-trending linear bands that continue for more than 30 km across the 3D seismic survey (Figs. 4B, 5B and 6B; Table 1). These linear bands are parallel to subparallel to the long axis of the Central submarine canyon with no evidence of divergent patterns (Figs. 4B, 5B, 6B and 11B; Table 1).

4.1.3 Seismic facies 3: Sheet-like chaotic seismic facies

In cross-sectional view, seismic facies 3 is composed of chaotic, low-amplitude, and semitransparent seismic reflections and exhibits sheet-like cross-sectional geometry (Fig. 6C; Table 1). It is bounded at its base by a laterally continuous, bed-parallel undeformed seismic reflector (Fig. 6C; Table 1). In plan view, it is represented by light- and dark-colored sheets (high and low coherence values, respectively) and occupies an area ranging from hundreds to thousands of square kilometers (Figs. 6B to 11B; Table 1).

4.1.4 Seismic facies 4: Landward dipping arcuate seismic facies

In plan form, seismic facies 4 is seen as extensive ridges of alternating light and dark colors and are seismically imaged as a corrugated irregular surface (Figs. 7B, 8B and 9B; Table 1). These closely spaced ridges are commonly parallel or subparallel to each other and show arcuate plan-view morphology with an orientation overall parallel or subparallel to the strike of the regional slope (Figs. 7B, 8B and 9B; Table 1). In cross-section, seismic facies 4 is made up of packages of parallel, steeply landward dipping reflections that are separated by offsets with up to 80 m relief (Figs. 7C and 9D; Table 1).

4.1.5 Seismic facies 5 and 6: Low- and high-coherence chaotic seismic facies

Low-coherence chaotic seismic facies (seismic facies 5) are represented by chaotic, low-amplitude, discontinuous seismic reflections, whereas high-coherence chaotic seismic facies (seismic facies 6) are made up of chaotic, low-amplitude moderate continuous seismic reflections (Fig. 8C; Table 1). In plan view, seismic facies 5 is seen as low-coherence sheets (light-colored areas in Figs. 6B to 11B; Table 1), whereas seismic facies 6 is expressed as high-coherence sheets (dark-colored areas in Figs. 6B to 11B; Table 1).

4.1.6 Seismic facies 7: Tapering-upward, block seismic facies

Seismic facies 7 consists of tapering-upward, moderate- to high-amplitude reflections with variable seismic reflection continuity (Fig. 9C; Table 1). In plan form, seismic facies 7 is up to 1.5 km wide and 120 m high and is seismically imaged as a corrugated irregular surface (Figs. 9B, 9C and 10B).

4.1.7 Seismic facies 8: Arcuate seismic facies

Seismic facies 8 are represented by a laterally continuous, undeformed reflection marking the upslope margin of MTCs, where the basal surface steps up to cut and intersect stratigraphically higher, chronostratigraphically younger slope stratigraphy (hot colored-shaded area in Fig. 10C; Table 1). In plan view, they appear as arcuate scarps oriented subparallel to the strike of the regional slope (Fig. 10B).

4.1.8 Seismic facies 9: Diverging lineation seismic facies

Seismic facies 9 appears as alternating high- and low-amplitude reflections with flat-bottomed cross-sectional geometry, which resemble a string of beads as seen in section view with basal truncation of around 10 m relief (Fig. 11C; Table 1). Each of these ‘beads’ is seen as a dark-colored single, narrow, northwest-southeast-trending tortuous incised scour (Fig. 11C). In plan view, they are expressed as radiating small-scour features that are continuous over 20 km in 3D coherence volumes (Fig.

11C; Table 1).

4.1.9 Seismic facies 10: Remnant seismic facies

Seismic facies 10 appear as discrete blocks of high-amplitude continuous reflections and exhibit irregular-shaped cross-sectional geometry with an irregular top and a bed-parallel base (Fig. 11D; Table 1). In cross-section, seismic facies 10 is represented as an undeformed ‘island’ surrounded by chaotic seismic facies (seismic facies 5 and 6). The ‘islands’ are seen as irregular-shaped, light-colored, single, north-south-trending blocks, are up to 45 m thick with a maximum long axis of 15 km (Fig. 11), and cover an area ranging from several square kilometers to a few tens of square meters (Figs. 11C and 11D; Table 1).

4. 2 Sedimentological interpretation

4.2.1 Seismic facies 1: Detached MTCs

Chaotic seismic facies 1 displays many of the recognition criteria typically used to recognize MTCs on seismic-reflection data (Moscardelli et al., 2006, 2012; Bull et al., 2009; Jackson, 2011, 2012; Olafiranye et al., 2013). Seismic facies 1 is further interpreted as detached MTCs, as discussed later (Fig. 4; Table 1).

4.2.2 Seismic facies 2: Striations

The overall seismic expression of seismic facies 2 shares many similarities with seismic reflection patterns of striations documented in many previous studies (Gee et al., 2005, 2006; Moscardelli et al. 2006; Bull et al. 2009; Jackson, 2011). Long linear seismic facies are therefore interpreted as striations (Figs. 4B, 5B, 5C and 6B; Table 1) that are differentiated from grooves due to the absence of downslope divergence

(Posamentier and Kolla, 2003; Moscardelli et al., 2006).

4.2.3 Seismic facies 3: Attached MTCs

The overall seismic reflection patterns of seismic facies 3 are wholly compatible with the recognition criteria of MTCs on seismic reflection data (Moscardelli et al., 2006, 2012; Bull et al., 2009; Jackson, 2011, 2012; Olafiranye et al., 2013). Where similar seismic facies have been documented, as in the Columbus Basin along offshore Trinidad and the Santos Basin along the offshore Brazil, they have been interpreted as the accumulation of mud-rich sediments (Shipp et al., 2004; Moscardelli et al., 2006; Jackson, 2012). Seismic facies 3 is further interpreted as attached MTCs (Fig. 6C and 6B to 11B; Table 1), as discussed below.

4.2.4 Seismic facies 4: Pressure ridges

Seismic facies 4 displays very similar seismic expression of pressure ridges that have been described at terminal ends of MTCs in Columbus, offshore Trinidad (Moscardelli et al., 2006), in the Norwegian continental slope (Bull et al., 2009) and in the Gulf of Mexico (Posamentier and Kolla, 2003). Packages of parallel, steeply landward dipping reflections as seen from this seismic facies are generally interpreted as thrusts coeval to the emplacement of the MTC (Bull et al., 2009) (Figs. 7B, 8B and 9B; Table 1). Examples of pressure ridges can be seen from MTC4, MTC5, and MTC6 (Figs. 7B, 8B and 9B; Table 1).

4.2.5 Seismic facies 5 and 6: Less and highly deformed MTCs

Seismic facies 5 and 6 are both expressed as chaotic, low-amplitude seismic reflections and exhibit many of the criteria used to identify MTCs (Moscardelli et al., 2006, 2012; Bull et al., 2009; Jackson, 2011, 2012). We follow the interpretation of Gamboa et al. (2010) who suggested that chaotic seismic facies displaying light colored coherent patterns (seismic facies 5 in this study) can be best considered as less deformed MTCs, whereas chaotic seismic facies exhibiting dark colored coherent patterns (seismic facies 6 in the current study) can be interpreted as highly deformed MTCs (for full details see Figs. 4C and 8C of Gamboa et al. 2010) (Figs. 6B to 11B; Table 1).

4.2.6 Seismic facies 7: Translated blocks

Based on similar features described from similar feature occurring within MTCs, seismic facies 7 is interpreted as translated blocks (Posamentier and Kolla, 2003; Gee et al., 2008; Bull et al., 2009; Jackson 2012; Table 1). MTC6 includes well-imaged examples of translated blocks (Figs. 9B, 9C and 10B; Table 1).

4.2.7 Seismic facies 8: Headwall escarpments

Seismic facies 8 exhibits a similar seismic expression to the headwall domain of a MTC in Columbus along offshore Trinidad (Moscardelli et al., 2006) and in Storegga Slide in Norwegian continental slope (Bull et al., 2009) (Figs. 10B and 10C; Table 1). Their arcuate plan-form geometries as seen in plan view differentiate them from tectonic normal faults, and previous work suggested that headwall escarpments formed in the same way as extensional faults (Bull et al., 2009).

4.2.8 Seismic facies 9: Cat-claw grooves

Similar feature described from other MTCs have interpreted radiating small-scour features (seismic facies 9 in this study) as basal grooves (Fig. 11C;

Table 1), also termed ‘cat-claw scours’ by Moscardelli et al. (2006), as evidence of abrupt changes in debris-flow conditions (Moscardelli et al., 2006; Bull et al., 2009) (Fig. 11B; Table 1). Similar radiating small-scour features were documented in offshore Brunei and are termed ‘monkey fingers’ by McGilvery and Cook (2003).

4.2.8 Seismic facies 10: Remnant blocks

Where similar seismic facies have been documented, as in Norwegian continental margin (Figs. 10C and 10D in Bull et al., 2009), offshore Espírito Santo, Brazil (Figs. 1B, 2A, 3A and 6A in Alves, 2010), an offshore Angola (Figs. 5 and 10 in Olafiranye et al., 2013), seismic facies of weakly deformed blocks of high-amplitude continuous reflections with irregular-shaped cross-sectional geometry were interpreted as remnant blocks or megaclasts (Jackson 2012) (Figs. 11C and 11D; Table 1).

5. General description of MTCs as documented in this case of the Qiongdongnan Basin along northwestern South China Sea margin

Eight separate MTCs, MTC1 to MTC8, were identified in the Qiongdongnan Basin. General descriptions of these eight MTCs are presented in Table 2 and are provided in this section.

5.1 General description of MTC1 and MTC2

The basal bounding surfaces of MTC1 and MTC2 show a U-shaped bathymetric confinement with a relief decreasing northeastward, resulting in a confined setting (Fig. 4A and 5A, respectively; Table 3). Both MTC1 and MTC2 are confined within the Central submarine canyon and are orientated subparallel to the strike of the regional slope (Figs. 1, 2, 4A and 5A). Morphologically, MTC1 and MTC2 cover an area of approximately 210 km^2 and 250 km^2, respectively (Table 2). The estimated volumes of remobilized sediments of MTC1 and MTC2 are about 9 km^3 and 15 km^3, respectively (Table 2). Both MTC1 and MTC2 show long striations at their base (Figs. 4B and 5B).

5.2 General description of MTC3, MTC4, MTC5 and MTC6

Three-dimensional perspective views of the basal bounding surfaces of MTC3, MTC4, MTC5 and MTC6 show a semi-confined setting that comprises an unconfined setting in the northern part of the study area and a confined setting in the southern part, above which these four MTCs occur (Fig. 6A to 9A; Table 3). MTC3 has an average thickness of approximately 110 m, the volume of remobilized sediments calculated for MTC3 is around 70 km^3 (Table 2). In plan view, it covers a region of about 700 km^2 and is composed of mainly of seismic facies 5 and 6, less and highly deformed MTCs (Figs. 4 to 11; Table 2). Sigmoid-oblique-progradational seismic facies located near palaeoshelf break occur above basal bounding surface of MTC3 (Fig. 2). They are composed of deformed, moderate to high amplitude and moderate to low continuous reflections with wedge-shaped geometries and exhibit clear, sigmoid-oblique progradational configurations (hot-colored areas in Fig. 2). They share affinities with shelf-edge deltas documented by Porebski and Steel (2003) and, when coupled with their locations on the shelf-slope profile and the deformed and disputed seismic reflection configurations, suggest that this seismic facies can be best interpreted as deformed shelf-edge deltas (Fig. 2).

MTC4 and MTC5 approximately cover similar areas, about 1100 km^2 (Table 2). Thicknesses of MTC4 and MTC5 are variable, reaching an average thickness of approximately 100 m (Table 2). Total volumes of MTC4 and MTC5 are calculated to be ～100 $km^3$and ～140 km^3, respectively (Table 2). Internally, MTC4 is characterized by widespread occurrence of well-imaged arcuate pressure ridges and consists predominantly of less deformed MTCs (Figs. 4B to 7B), whereas highly deformed MTCs and pressure ridges (Fig. 8B) widely developed in MTC5. MTC6 occupies an approximate area of ～1200 km^2, and the thickness of MTC6 is variable, reaching an average thickness of ～80 m (Table 2). MTC6 consists of 90 km^3 remobilized sediments and contains pressure ridges, translated blocks and show striations at their base (Figs. 9B and 9D; Table 2).

5.3 General description of MTC7 and MTC8

MTC7 and MTC8 developed in an unconfined setting with a southeastward decrease in relief (Figs. 10A and 11A; Tables 2 and 3). MTC7 and MTC8 cover an area of approximately 800 km^2 and 1100 km^2, respectively (Figs. 10A and 11A; Table 3). The thickness of MTC7 is also variable, reaching an average thickness of about 70 m, and the total volume of remobilized sediments of MTC7 is calculated to be about 55 km^3 (Table 2). An estimated volume of 50 km^3 remobilized sediments was transported from the continental shelf and/or upper slope to the region where MTC8 developed (Table 2). Internally, MTC7 consists of high and less deformed facies contains translated blocks (Fig. 10B), whereas MTC8 comprises basal cat-claw grooves, translated blocks, ,and remnant blocks and is composed of highly and less deformed MTCs (Figs. 11B, 11C and 11D).

6 The origin and classification of MTCs as documented in the case of the Qiongdongnan Basin

6.1 Source areas of MTCs as documented in the case of the Qiongdongnan Basin

6.1.1 Source areas of MTC1 and MTC2

MTC1 and MTC2 are totally confined within the Central submarine canyon (the U-shaped confinement with the northeastward decrease in relief as presented in Figs 4A and 5A). Gong et al. (2011) suggested large-scale and high-energy sediment gravity flows were the dominant processes within the Central submarine canyon around the time of MTC1 and MTC2 emplacement. Sediment gravity currents flowing along the long axis of the Central submarine canyon are interpreted to have induced small collapses and local instabilities on canyon margins, resulting in small-scale mass-wasting processes and resultant MTCs composed of collapsed sediments derived from canyon margins, suggesting that MTC1 and MTC2 are likely fed by localized source areas (Table 3).

In addition, MTC1 and MTC2 show long striations at their base (Figs. 5B and 6B), which trend along the long axis of the Central submarine canyon. According to Bull et al. (2009), striations directly record the translation of MTC body across the basal bounding surfaces and are indicative of transport direction of debris flow processes. The trend of striations occurring in MTC1 and MTC2 as shown in Figs. 5B and 6B suggests a transport direction along the long axis of the Central submarine canyon for MTC1 and MTC2. This suggests that MTC1 and MTC2 most likely originated from collapses of the studied slope that were triggered by regional tectonic events as discussed later (Table 3).

6.1.2 Source areas of MTC3 to MTC8

MTC3 and MTC6 are linked with deformed shelf-edge deltas and occur immediately basinward of these deformed shelf-edge deltas (Fig. 2). The repaid progradation of shelf-edge deltas can lead to the development of gravitational instabilities and large-scale sediment failures in the distal part of shelf-edge deltas as the delta slope merges with the basin margin slope. This is expressed by disrupted and deformed seismic reflection configurations as seen from the terminal end of shelf-edge deltas (Fig. 2). These observations would support the interpretation that deformed shelf-edge deltas are source area of MTC3 and MTC6 (Fig. 2, Table 3).

Below basal bounding surfaces of MTC4, MTC5 and MTC8 (BS4, BS5 and BS8) there are clear truncation terminations occurring on the continental shelf (yellow dots in Fig. 2), implying that the subaerial exposure and erosion of continental shelves and/or shelf margins were common during the deposition of MTC4, MTC5 and MTC8. These processes in turn supplied sediments for deep-water settings where MTC4, MTC5 and MTC8 occur and, when coupled with the fact that MTC4, MTC5 and MTC8 occur immediately basinward of shelf edges, support the interpretation that MTC4, MTC5 and MTC8 were probably fed by sediments derived from continental shelf and/or shelf margins (Table 3).

MTC7 occurs immediately seaward of extensive headwall escarpments recognized in the northern part of the study area (Figs. 2, 10B and 10C). Bull et al.

(2009) suggested that the orientation of the headwall escarpment is consistent with the initial direction of mass-wasting processes. According to this hypothesis, the initial transport direction of MTC7 was downslope to the south and is parallel to the orientation of the headwall escarpment as presented in Fig. 10B, suggesting that source area for MTC7 lies in the upper slope (Table 3).

6.2 Classification of MTCs as documented in the case of the Qiongdongnan Basin

From a sedimentological perspective, Moscardelli and Wood (2008) proposed that MTCs can be classified as detached and attached types, considering their triggering mechanisms and relationships to source area. This classification is employed to classify MTCs documented in this study. MTC1 and MTC2 are classified as ‘detached MTCs’, considering the fact that they are areally confined within the Central submarine canyon and were fed neither by continental shelves or upper slopes, but rather by canyon margins (Table 3).

The other five MTCs (MTC3 to MTC6, and MTC8), in contrast, all extend from their shelf margins or shelf-edge delta sources to the deep-water basin (Table 3), all of which can be classified as ‘shelf-attached MTCs’ (Table 3). The upper slope of the studied margin is the source area of MTC7, suggesting that MTC7 can be classified as ‘slope-attached MTC’ (Table 3).

7 Triggering mechanisms of MTCs documented in the Qiongdongnan Basin

Many previous studies suggested that MTCs can be triggered by a number of mechanisms and triggers, including high sedimentation rates, the gas-hydrate dissolution, sea-level fluctuations, tectonics, seafloor oversteepening, overpressures, earthquakes, etc. (Solheim et al., 2005; Moscardelli et al., 2006; Strozyk et al., 2009; Gamberi et al., 2011; Jackson, 2011, 2012; Mosher and Cambell, 2011; Riedel et al., 2012, among others). The current study suggests that a combination of factors, as discussed below, contributed to the initiation and development of MTCs documented in the current case study (Table 3).

7.1 Triggering mechanisms of detached MTCs

7.1.1 Paleo-seafloor morphology

Gong et al. (2011) suggested that slope-subparallel bathymetric confinement (the Central submarine canyon) predated the development of detached MTCs (Figs. 4 and 5). No.2 Fault and other basement faults are oriented subparallel to the strike of the regional slope (Figs. 1 and 2). Both the slope-subparallel bathymetric confinement and slope-subparallel faults most likely acted as a strong physiographic 'container' (the Central submarine canyon) to constrain mass-wasting processes responsible for the formation of detached MTCs, resulting in MTC1 and MTC2 that are oriented subparallel to the strike of the regional slope and are areally confined within the bathymetric confinement (Figs. 1 to 5).

7.1.2 Regional tectonic events

The study area is bounded to the west by the Red River Fault and to the east by No. 2 Fault (Figs. 1 and 2), both of which shifted from sinistral to dextral movement at about 5.5 Ma (Xie et al., 2008; Zhu et al., 2009, 2011) (Fig. 1). As suggested by Gong et al. (2011), the structural inversion of the Red River Fault and No. 2 Fault and associated tectonic activity most likely triggered small-small slope instability and localized collapses of the continental slope of the studied margin. The collapsed sediments were transported downcanyon through small-scale mass-wasting processes that were confined with the Central submarine canyon, resulting in localized MTCs (MTC1 and MTC2) (Figs. 2 to 5). In addition, these small-scale mass-wasting processes probably ‘ploughed’ the basal bounding surfaces of MTC1 and MTC2, yielding long striations (long linear seismic facies seen in plan-view geomorphic images presented in Figs. 4B and 5B) oriented parallel to the long axis of the Central submarine canyon.

7.1.3 Canyon margin oversteepening

These energetic sediment gravity flows induced by regional tectonic events flowing along the long axis of the slope-subparallel bathymetric confinement (the Central submarine canyon) could provide sufficient shear stress to flush the canyon and erode canyon margins significantly. Canyon margins might become oversteepened and collapse due to the significant erosion of canyon margins (e.g. Hodgson et al. 2011). This in turn further contributed to the development of detached MTCs (MTC1 and MTC2) consisting of sediments derived from canyon walls. Similar canyon-margin-failure trigger mechanisms have been invoked by Moscardelli and Wood (2008) from their 3D seismic case study from the Columbus Basin, offshore Trinidad.

7.2 Triggering mechanisms of attached MTCs

7.2.1 High sedimentation rates, rapid slope progradation and slope oversteepening

Zhu et al. (2011) suggested that sedimentation rates from Pliocene (5.5 Ma) to Quaternary in the Qiongdongnan Basin study area ranged from 400-800 m/My. This high sedimentation rate in turn most likely resulted in rapid progradation of the basin margin. This can be evidenced by the fact that shelf edges of the study area migrated seaward for more than 50 km from Pliocene to present (Gong et al., 2011). In response to the rapid progradation of the basin margin, the slope would become oversteepened, as suggested by the fact that the average slope gradient of the study area reach up to 4° to 6° (Fig. 2). All of these triggers probably induced gravitational instabilities and catastrophic collapses of shelf margins and/or upper slopes, resulting in large-scale mass-wasting processes and their associated attached MTCs (Table 3).

7.2.2 Rapid progradation of shelf-edge deltas

High sedimentation rates resulted in rapid progradation of shelf-edge deltas and, when coupled with other slope-failure triggers (e.g., ground motion, gas hydrate dissociation, sea level fluctuation, etc.) probably induced gravitational instabilities and large-scale sediment failures in the distal part of shelf-edge deltas (Figs. 2 and 4). This can be evidenced by the disrupted and deformed seismic reflection configurations as seen from the terminal end of sigmoid-oblique-progradational seismic facies (hot color-shaded areas in Fig. 2). It is likely that rapid progradation of shelf-edge deltas onto the upper slope would have contributed to the development of shelf-attached MTCs (Fig. 2; Table 3). Similar mechanisms triggering the development of shelf-attached MTCs fed by paleoshelf edge deltas have also been documented by Moscardelli and Wood (2008).

7.2.3 Tectonic activity and resultant seismicity

As discussed previously, the Red River Fault, No. 2 Fault and other basement experienced dextral movement from Pliocene to present, all of which caused high-frequency seismicity in the northern South China Sea margin (Zhu et al., 2009, 2011). Seismicity associated with this dextral movement have been documented in China, northern South China Sea margin, and the eastern Vietnam, etc. (Zhu et al., 2011). The tectonic activity and associated seismicity, coupled with other triggering mechanisms as stated above, most likely triggered extensively catastrophic collapses of continental shelves, shelf margins, shelf-edge deltas, or upper slopes by seismic shaking, forming large-scale mass-wasting processes and their associated attached MTCs as documented in this case (MTC3 to MTC8) (Table 3).

8. Lateral and vertical relationships with interstratified reservoirs

A seismic facies is made up of thalweg high-amplitude elements (the hot color-shaded area in Fig. 12), consisting of high amplitude reflections ('HARs', *sensu* Flood et al., 1991). HARs are contained within U-shaped basal erosional surface, across which there are clear truncation terminations below and onlap terminations above (Fig. 12). In plan view, they are expressed as high-amplitude and high-RMS-attribute zones with irregular-shaped morphology (hot color-shaded areas in Fig. 13). High-amplitude reflections confined within submarine canyons are commonly interpreted as channel fills (Manley et al., 1997; Mayall et al., 2006; Cross et al., 2009). Where similar seismic facies have been calibrated with borehole data, as in the Amazon fans, they have proved to correspond to coarse channel-lag material (Manley et al., 1997).

MTCs are commonly considered as poor reservoirs and may serve as excellent seals (Moscardelli et al., 2006; Weimer and Slatt, 2007; Zhu et al., 2011). In cross-section, channel fills are blanketed and overlain by low-permeability and low-porosity MTCs (MTC1, MTC2 and MTC3) (Fig. 12). In plan view, channel fills are surrounded by MTCs (hot color-shaded areas in Figs. 13). MTC-related stratigraphic traps could form, provided that these channel fills are charged by deeper source rocks through hydrocarbon migration pathways and that the MTCs (MTC1, MTC2 and MTC3) act as lateral and top seals and prevent hydrocarbons from leaking out. MTC-related stratigraphic traps as recognized the current case study occupy an area of ca. 37 km^2 (hot color-shaded areas in Figs. 12 and 13). This type of stratigraphic trap may be common and represent potential drilling targets on many other MTC-bearing continental margins.

9. Conclusions

This study integrates plan-view geomorphic images of previously undocumented MTCs with detailed seismic facies characterization of these MTCs to document their stratigraphic architecture, seismic geomorphology, triggering mechanisms, and exploration significance.

(1) Eight MTCs, MTC1 to MTC8, were identified and are classified as detached and attached MTCs. Detached MTCs developed within bathymetric confinement occupy areas of hundreds of km^2 and consist of tens of km^3 of remobilized sediments. Attached MTCs occurring within semi-confined or unconfined settings are areally extensive (hundreds to thousands of km^2) and consist of few tens to few hundreds of km^3 remobilized sediments.

(2) Internally, detached MTCs display irregular cross-sectional geometry and contain long linear striations, whereas attached MTCs exhibit sheet-like cross-sectional geometry, consist mainly of weakly and highly deformed MTC materials and contain headwall escarpments, translated blocks, remnant blocks, pressure ridges, striations and cat-claw grooves.

(3) Detached MTCs resulted from small-scale mass-wasting processes induced by regional tectonic events and gravitational instabilities on canyon margins. Attached MTCs, in contrast, were created by large-scale mass-wasting processes triggered by high sedimentation rates, slope oversteepening, rapid progradation of shelf-edge deltas, tectonic activity and seismicity.

(4) From a sedimentological perspective, this study documents stratigraphic

architecture, seismic geomorphology and triggering mechanisms of two different types of MTCs, contributing to a better understanding of the range and distribution of MTCs.

(5) From a hydrocarbon exploration perspective, our work suggests that detached MTCs could create MTCs-related stratigraphic traps that may be common and probably represent potential drilling targets in deep-water basins, helping to identify MTC-related hydrocarbon traps on continental margins.

Acknowledgments

We are grateful to CNOOC for providing the data and for its permission to publish the results of this study. We thank Editor Yongtai Yang, and two reviewer, Dr. Lorena Moscardelli and Dr. Michael Riedel, for taking time to plough through an earlier version and make numerous constructive comments that significantly improved this paper. We thank the Associate Editor of Marine and Petroleum Geology, Johannes Wendebougr, and two anonymous reviewers for their critical but constructive reviews that significantly improved the quality of this contribution. This study was jointly supported by the National Basic Research Program of China (No. 2009CB219407), the National Natural Science Foundation of China (No. 41372115, No. 41302147 and No. 1304111), and the Science Foundation of China University of Petroleum, Beijing (No. 2462013YXBS001). The first author wish to thank Tao Wang (former minister of the Ministry of Petroleum Industry of the People's Republic of China), State Key Laboratory of Petroleum Resources and Prospecting (China University of Petroleum, Beijing), and China University of Petroleum (Beijing) for their support of C. Gong's PhD research and studies.

References

Alves, T.M., 2010. 3D Seismic examples of differential compaction in mass-transport deposits and their effect on post-failure strata. Marine Geology 271, 212–224.

Bull, S., Cartwright, J., Huuse, M., 2009. A review of kinematic indicators from mass-transport complexes using 3D seismic data. Marine and Petroleum Geology 26, 1132–1151.

Canals, M., Lastras, G., Urgeles, R., Casamor, J.L., Mienert, J., Cattaneo, A., De Batist, M., Haflidason, H., Imbo, Y., Laberg, J.S., Locat, J., Long, D., Longva, O., Masson, D.G., Sultan, N., Trincardi, F., Bryn, P., 2004. Slope failure dynamics and impacts from seafloor and shallow sub-seafloor geophysical data: case studies from the COSTA project. Marine Geology 213, 9–72.

Cross, N.E., Cunningham, A., Cook, R.J., Taha, A., Esmaie, E. and Swidan, N.E., 2009. Three-dimensional seismic geomorphology of a deep-water slope-channel system: The Sequoia field, offshore west Nile Delta, Egypt. AAPG Bulletin 93, 1063–1086.

Evans, D., Harrison, Z., Shannon, P.M., Laberg, J.S., Nielsen, T., Ayers, S., Holmes, R., Hoult, R.J., Lindberg, B., Haflidason, H., Long, D., Kuijpers, A., Andersen, E.S., Bryn, P., 2005. Palaeoslides and other mass failures of Pliocene to Pleistocene age along the Atlantic continental margin of NW Europe. Marine and Petroleum Geology 22, 1131–1148.

Gamberi, F., Rovere, M., Marani. M., 2011. Mass-transport complex evolution in a tectonically active margin (Gioia Basin, Southeastern Tyrrhenian Sea). Marine Geology 279, 98–110.

Gamboa, D., Alves, T., Cartwright, J., Terrinha, P., 2010. Mass-transport deposits distribution on a ‘passive’ continental margin: the Espírito Santo Basin (SE Brazil) during the Palaeogene. Marine and Petroleum Geology 27 (7), 1311–1324.

Gee, M.J.R., Gawthorpe, R.L., Friedmann, J.S., 2005. Giant striations at the base of a submarine landslide. Marine Geology 214, 287–294.

Gee, M.J.R., Gawthorpe, R.L., Friedmann, S.J., 2006. Triggering and evolution of a giant landslide, offshore Angola revealed by 3D seismic stratigraphy and geomorphology. Journal of Sedimentary Research 76, 9–19.

Gee, M.J.R., Uy, H.S., Warren, J., Morley, C.K., Lambiase, J.J., 2008. The Brunei slide: a giant submarine landslide on the North West Borneo Margin revealed by seismic data. Marine Geology 246, 9–23.

Gong, C., Wang, Y., Zhu, W., Li, W., Xu, Q., Zhang J.M., 2011. The Central submarine canyon in the Qiongdongnan Basin, northwestern South China Sea: Architecture, sequence stratigraphy, and depositional processes. Marine and Petroleum Geology 28, 1690–1702.

Gong, C., Wang, Y., Zhu, W., Li, W., Xu, Q., 2013. Upper Miocene to Quaternary unidirectionally migrating deep-water channels in the Pearl River Mouth Basin, northern South China Sea. AAPG Bulletin 97, 285–308.

Hodgson D.M., Di Celma C.N., Brunt R.L., Flint S.S., 2011, Submarine slope degradation and aggradation and the stratigraphic evolution of channel-levee systems, Journal of the Geological Society, 168, 625-628.

Jackson, C.A-L., 2012. The initiation of submarine slope failure and the emplacement of mass transport complexes in salt-related minibasins: A three-dimensional seismic-reflection case study from the Santos Basin, offshore Brazil. GSA Bulletin 124, 746–761.

Jackson, C.A-L., 2011. Three-dimensional seismic analysis of megaclast deformation within a mass transport deposit; implications for debris flow kinematics. Geology 39, 203–206.

Loucks, R.G., Kerans, C., Janson, X., Rojano, M.A.M., 2011. Lithofacies analysis and stratigraphic architecture of a deep-water carbonate debris apron: Lower Cretaceous (latest Aptian to latest Albian) Tamabra Formation, Poza Rica Field Area, Mexico. In: Shipp, R.C., Weimer, P., and Posamentier, H. (Eds.), Mass-transport Deposits in Deepwater Settings. SEPM Special Publications, vol. 96, pp. 67–390.

Manley, P.L., Pirmez, C., Busch, W. Cramp, A., 1997. Grain-size characterization of Amazon Fan deposits and comparison to seismic facies units. In: Flood, R.D., Piper, D.J.W., Klaus, A. and Peterson, L.C. (Eds), Proceedings of the Ocean Drilling Program, Scientific Results. 155, pp. 35–52.

Mayall, M., Jones, Ed., Casey, M., 2006. Turbidite channel reservoirs e key elements in facies prediction and effective development. In: Casey, M. (Ed.), Marine and Petroleum Geology, 23, pp. 821–841.

Moscardelli, L., Wood, L., Mann, P., 2006. Mass-transport complexes and associated processes in the offshore Area of Trinidad and Venezuela. AAPG Bulletin 90, 1059–1088.

Moscardelli, L., Wood, L., 2008. New classification system for mass-transport complexes in offshore Trinidad. Basin Research 20, 73–98.

Moscardelli, L., Hordbach, M., Wood, L.J., 2010. Tsunamigenic risk associated with mass transport complexes in offshore Trinidad and Venezuela. In: Mosher, D.C., Shipp, R.C., Moscardelli, L., Chaytor, J.D., Baxter, C.D.P., Lee, H.J., and Urgeles, R. (Eds.), Submarine Mass Movements and Their Consequences: 4th International Symposium. Springer, pp. 733–744.

Mosher, D.C., Moscardelli, L., Shipp, R.C., Chaytor, J.D., Baxter, C.D.P., Lee, H.J., Urgeles, R., 2010. Submarine mass movements and their consequences. In: Mosher, D.C., Shipp, R.C., Moscardelli, L., Chaytor, J.D., Baxter, C.D.P., Lee, H.J., and Urgeles, R. (Eds.), Submarine Mass Movements and Their Consequences: 4th International Symposium - Advances in Natural and Technological Hazards Research: Springer, v. 28, pp. 1–8.

Moscardelli, L., Wood, L., Dunlap, D.B., 2012. Shelf-edge deltas along structurally complex margins: A case study from eastern offshore Trinidad. AAPG Bulletin 96, 1483–1522.

Mosher, Cambell, D.C., 2011. The Barrington submarine mass-transport deposits, western Scotian Slope, Canada. In: Shipp, C., Weimer, P., and Posamentier, H. (Eds.), Submarine slope systems. SEPM Special Publications, 96, 151–161.

Olafiranye, K., Jackson, C.A.-L., Hodgson, D.M., 2013. The role of tectonics and mass-transport complex emplacement on upper slope stratigraphic evolution: A 3D seismic case study from offshore Angola. Marine and Petroleum Geology 44, 196–216.

Porebski, S.J., Steel, R.J., 2003. Shelf-edge deltas: Their stratigraphic significance and relation to deepwater sands. Earth Science Review 62, 283–326.

Posamentier, H.W., Kolla,V., 2003. Seismic geomorphology and stratigraphy of depositional elements in deep-water settings. Journal of Sedimentary Research 73, 367–388.

Posamentier, H.W., Davies, R.J., Cartwright, J.A., Wood, L.J., 2007, Seismic geomorphology: An overview. In: Davies, R.J., Posamentier, H.W., Wood, L.J., and Cartwright, J.A. (Eds), Seismic geomorphology: Applications to hydrocarbon exploration and production. Geological Society (London) Special Publication, vol, 277, pp. 1–14.

Richardson, S.E.J., Davies, R.J., Allen, M.B., Grant, S.F., 2011. Structure and evolution of mass transport deposits in the South Caspian Basin, Azerbaijan. Basin Research 23, 702–719.

Riedel, M., Bahk, J.-J., Scholz, N.A., Ryu, B.-J., Yoo, D.-G., Kim, W., Kim, G.Y., 2012.

Mass-transport deposits and gas hydrate occurrences in the Ulleung Basin, East Sea e Part 2: Gas hydrate content and fracture-induced anisotropy. Marine and Petroleum Geology 35, 75–90.

Shipp, R.C., Nott, J.A., Newlin, J.A., 2004. Physical characteristics and impact of mass-transport complexes on deepwater jetted conductors and suction anchor piles. Offshore Technology Conference, Houston, Texas.

Shipp, R.C., Lu, H., 2011. Impact of a large mass-transport deposit on a field development in the upper slope of southwestern Sabah, Malaysia, offshore northwest Borneo. In: Shipp, R.C., Weimer, P., and Posamentier, H. (Eds.), Mass-transport Deposits in Deepwater Settings. SEPM Special Publications, vol. 96, pp. 199–220.

Shipp, R.C., Weimer, P., Posamentier, H.W., 2011. Mass-transport deposits in deepwater settings: An introduction. In: Shipp, R.C., Weimer, P., and Posamentier, H. (Eds.), Mass-transport Deposits in Deepwater Settings. SEPM Special Publications, vol. 96, pp. 3–6.

Solheim, A., Berg, K., Forsberg, C.F., Bryn, P., 2005. The Storegga Slide complex: repetitive large scale sliding with similar cause and development. Marine and Petroleum Geology 22, 97–107.

Strozyk, F., Huhn, K., Strasser, M., Krastel, S., Kock, I ., Kopf, A., 2009. New evidence for massive gravitational mass-transport deposits in the southern Cretan Sea, eastern Mediterranean. Marine Geology 263, 97–107.

Vail, P.R., Mitchum, R.M., Thompson, S., 1977. Seismic stratigraphy and global changes of sea level, part 3: Relative changes of sea level from coastal onlap. In: Payton, C.E., (Eds.), Seismic stratigraphy applications to hydrocarbon exploration: AAPG Memoir 26, pp. 63–82.

Weimer, P., Slatt, R.M., 2007. Introduction to the petroleum geology of deep-water settings. AAPG Memoir, 419–456.

Weimer, P., Shipp, C., 2004. Mass-transport complexes: Musing on past uses and suggestions for future directions. Offshore Technology Conference, Houston, Texas.

Xie, X., Muller, R.D., Li, S., Gong, Z., Steinberger, B., 2006. Origin of anomalous subsidence along the Northern South China Sea margin and its relationship to dynamic topography. Marine and Petroleum Geology 23, 745–765.

Xie, X., Muller, R.D., Ren, J., Jiang, T., Zhang, C., 2008. Stratigraphic architecture and evolution of the continental slope system in offshore Hainan, northern continental margin of the South China Sea. Marine Geology 247, 129–144.

Zhu, M., Graham, S.A., Mchargue, T., 2009. The Red River Fault zone in the Yinggehai Basin, South China Sea. Tectonophysics 476, 397–417.

Zhu, M., McHargue, T., Graham, S.A., 2011. 3D seismic-reflection characterization of submarine slides on a Pliocene siliciclastic continental slope and its implications for tectonics, sediment supply, and climate change, South China Sea. In: Shipp, R.C., Weimer, P., and Posamentier, H. (Eds.), Mass-transport Deposits in Deepwater Settings. SEPM Special Publications, vol. 96, pp. 111–126.

Table 1 Seismic facies description and interpretation

Seismic facies	Plan-view appearance		Cross-sectional seismic expression				Sedimentological interpretations
	Appearance	Seismic examples	Amplitude	Continuity	Cross-sectional geometry	Seismic examples	
Seismic facies 1: Irregular-shaped chaotic seismic facies	Irregular shape	Fig. 4C	Low	Variable	Irregular shaped	Fig. 4C	Detached MTCs
Seismic facies 2: Long linear seismic facies	Long linear bands	Figs. 5C and 6C	Variable	Discontinuous	V shaped	Fig. 5C	Striations
Seismic facies 3: Sheet-like chaotic seismic facies	Sheet-like beds	Figs. 6Cand 11C	Low	Variable	Sheet like	Fig. 6C	Attached MTCs
Seismic facies 4: Arcuate seismic facies	Arcuate ridges	Figs. 7C, 8C and 9D	Low	Variable	Landward dipping	Figs. 7C and 9D	Pressure ridges
Seismic facies 5: Low-coherence chaotic seismic facies	Low-coherence sheets	Fig. 8C	Low	Discontinuous	Sheet like	Fig. 8C	Less deformed MTCs
Seismic facies 6: High-coherence chaotic seismic facies	High-coherence sheets	Fig. 8C	Low	Moderate	Sheet like	Fig. 8C	Highly deformed MTCs
Seismic facies 7: Tapering-upward, block seismic facies	Corrugated irregular surface	Fig. 9C	Moderate to high	Variable	Tapering upward	Fig. 9C	Translated blocks
Seismic facies 8: Headwall seismic facies	Irregular, continuous scarps	Fig. 10C	High	Continuous	Seen as a scarp or boundary	Fig. 10C	Headwall escarpments
Seismic facies 9: Cat-claw seismic facies:	Radiating small-scour features	Fig. 11C	Variable	Discontinuous	Seen as a string of beads	Fig. 11C	Cat-claw grooves
Seismic facies 10: Remnant seismic facies:	Irregular-shaped blocks	Fig. 11C	High	Continuous	Irregular shaped	Fig. 11D	Remnant blocks

Table 2 Morphological characteristics of eight separate MTCs, MTC1 to MTC8, as documented in the case of the Qiongdongnan Basin along the northwestern South China Sea margin. The 'MTC areas', 'MTC thicknesses' and 'MTC volumes' were calculated within the limits of the 3-D seismic survey.

MTC	Area (km^2)		Mean thickness (m)	Volume (km^3)		Distribution	
MTC1	～210	100s	～120	～9	10s	Confined within canyon	Subparallel to slope
MTC2	～250		～115	～15		Confined within canyon	
MTC3	～700	1000s	～110	～70	From 10s to 100s	～40% of the study area	Upper slope to deep basin
MTC4	～1000		～100	～100		～65% of the study area	
MTC5	～1000		～110	～140		～65% of the study area	
MTC6	～1200		～80	～90		～70% of the study area	
MTC7	～800		～70	～55		～50% of the study area	Mid slope to deep basin
MTC8	～1100		～50	～50		～65% of the study area	Upper slope to deep basin

Table 3 The classification, depositional topography, source area, and causal mechanisms of eight separate MTCs as documented in the case of Qiongdongnan Basin along the northwestern South China Sea margin.

MTCs	Depositional topography	Source area	Classification		Triggering mechanisms
MTC1	Topographic confinement	Canyon margins	Detached MTCs		Local instabilities on canyon margins and regional tectonic events
MTC2	Topographic confinement	Canyon margins			
MTC3	Semi-confined settings	Shelf-edge deltas	Attached MTCs	Shelf-attached MTCs	High sedimentation rates
MTC4	Semi-confined settings	Continental shelves			Rapid shelf-edge deltas progradation
MTC5	Semi-confined settings	Continental shelves			Rapid slope progradation
MTC6	Semi-confined settings	Shelf-edge deltas			Slope over steepening
MTC7	Unconfined settings	Upper slopes		Slope-attached MTCs	Tectonics activities and associated seismicity
MTC8	Unconfined settings	Continental shelves		Shelf-attached MTCs	

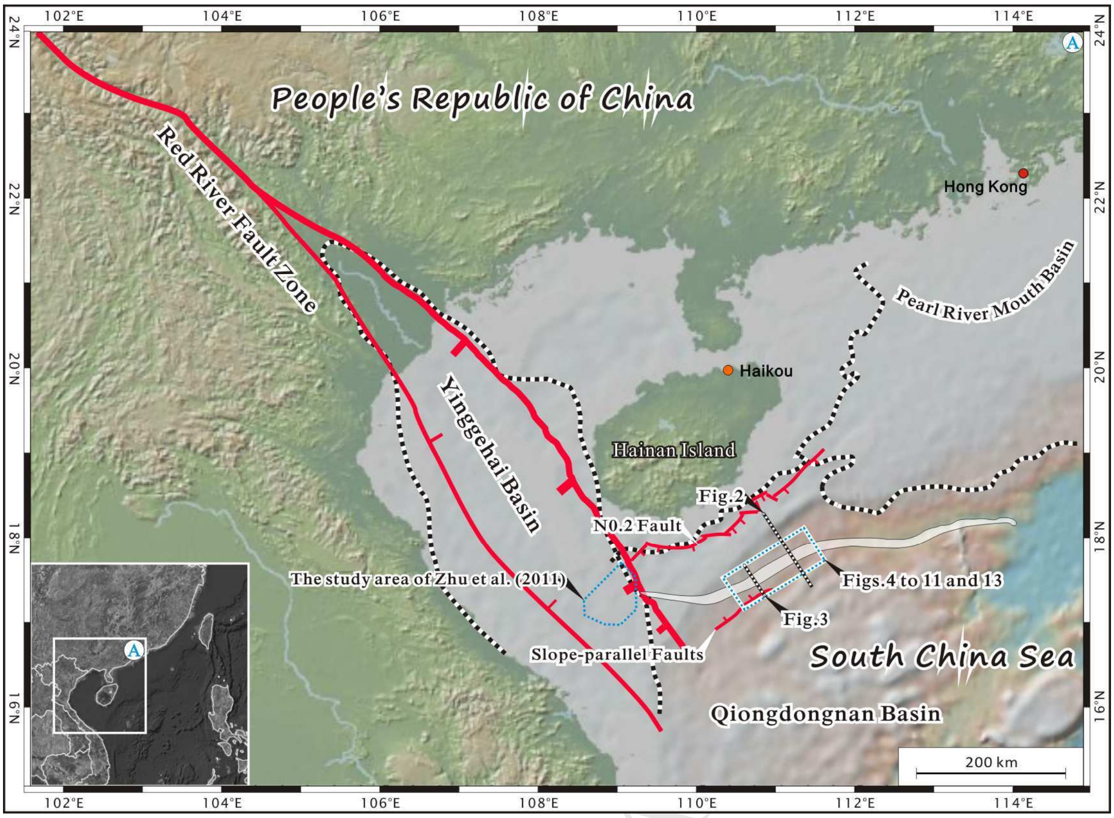

Figure 1. Bathymetric map showing morphological characteristics of the study area and plan-view locations of dip-oriented regional seismic transects presented in Figs. 2 and 3. Major structure features are modified from Xie et al. (2008) and Zhu et al. (2011). Two-way traveltime (TWTT) structural maps (Figs. 4A to 11A), plan-view geomorphic images derived from 3D coherence volumes (Figs. 4B to 11B), 3D seismic amplitude (Fig. 13A) and RMS attribute volumes (Fig. 13B) cover the full 3D seismic survey marked by the rectangle with dotted outline.

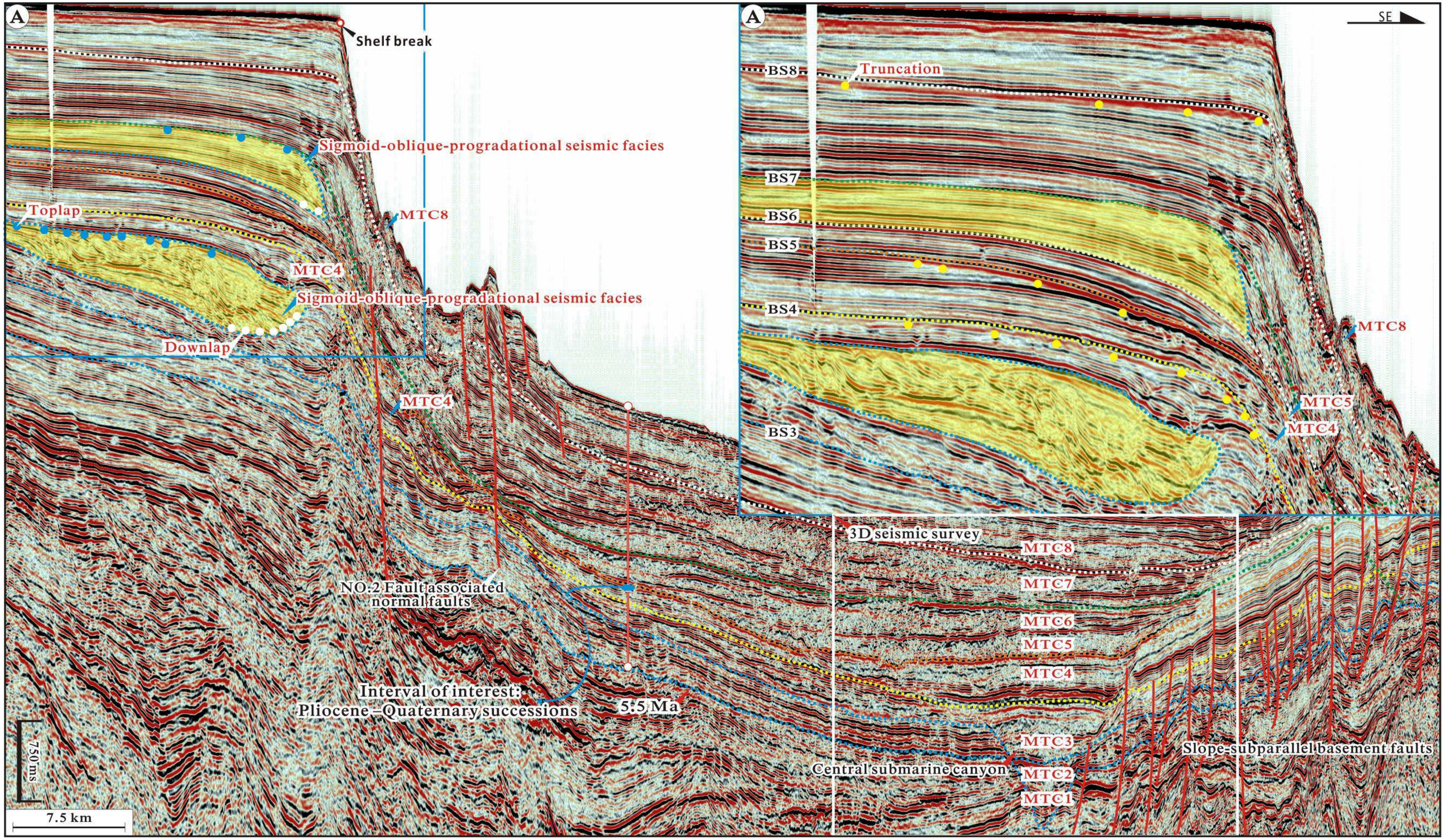
A
Shelf break
Sigmoid-oblique-progradational seismic facies
Toplap
MTC8
MTC4
Sigmoid-oblique-progradational seismic facies
Downlap
MTC4
NO.2 Fault associated normal faults
Interval of interest: Pliocene –Quaternary successions
5.5 Ma
750 ms
7.5 km
A
SE
BS8
Truncation
BS7
BS6
BS5
BS4
BS3
MTC8
MTC5
MTC4
3D seismic survey
MTC8
MTC7
MTC6
MTC5
MTC4
MTC3
Central submarine canyon
MTC2
MTC1
Slope-subparallel basement faults

Figure 2. Dip-oriented seismic traverses (for line location see Fig.1) across the entire studied margin showing stratigraphic architecture and cross-sectional seismic expression of eight successive MTCs (MTC1 to MTC8) and deformed shelf-edge deltas seen as sigmoid-oblique-progradational seismic facies (hot color-shaded areas). BS = Basal bounding surfaces.

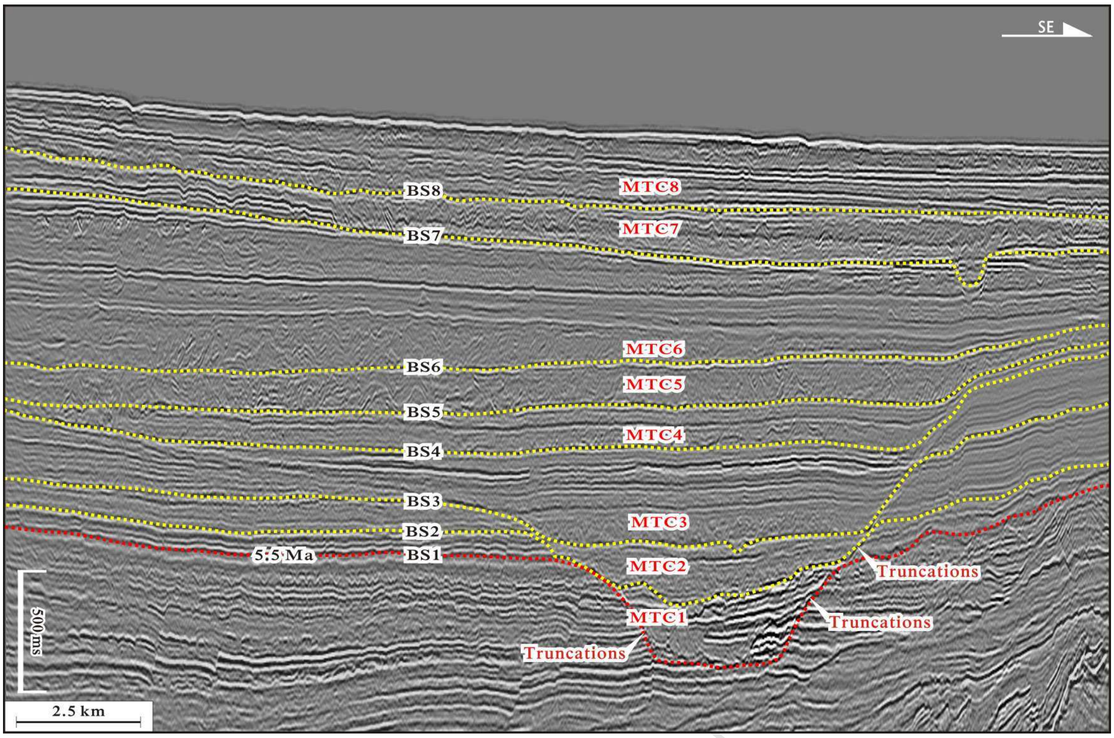

Figure 3. Two-dimensional seismic section from three-dimensional seismic volume (see Fig. 1 for line location) showing cross-sectional seismic expression of eight successive MTCs, MTC1 to MTC8, developed within the Pliocene-Quaternary sedimentary interval in the Qiongdongnan Basin. These eight MTCs are characterized by transparent, chaotic reflection packages with variable seismic amplitude and reflection continuity. Please refer to Fig. 1 for the plan-view location of the seismic traverse presented in this figure. BS = Basal bounding surfaces.

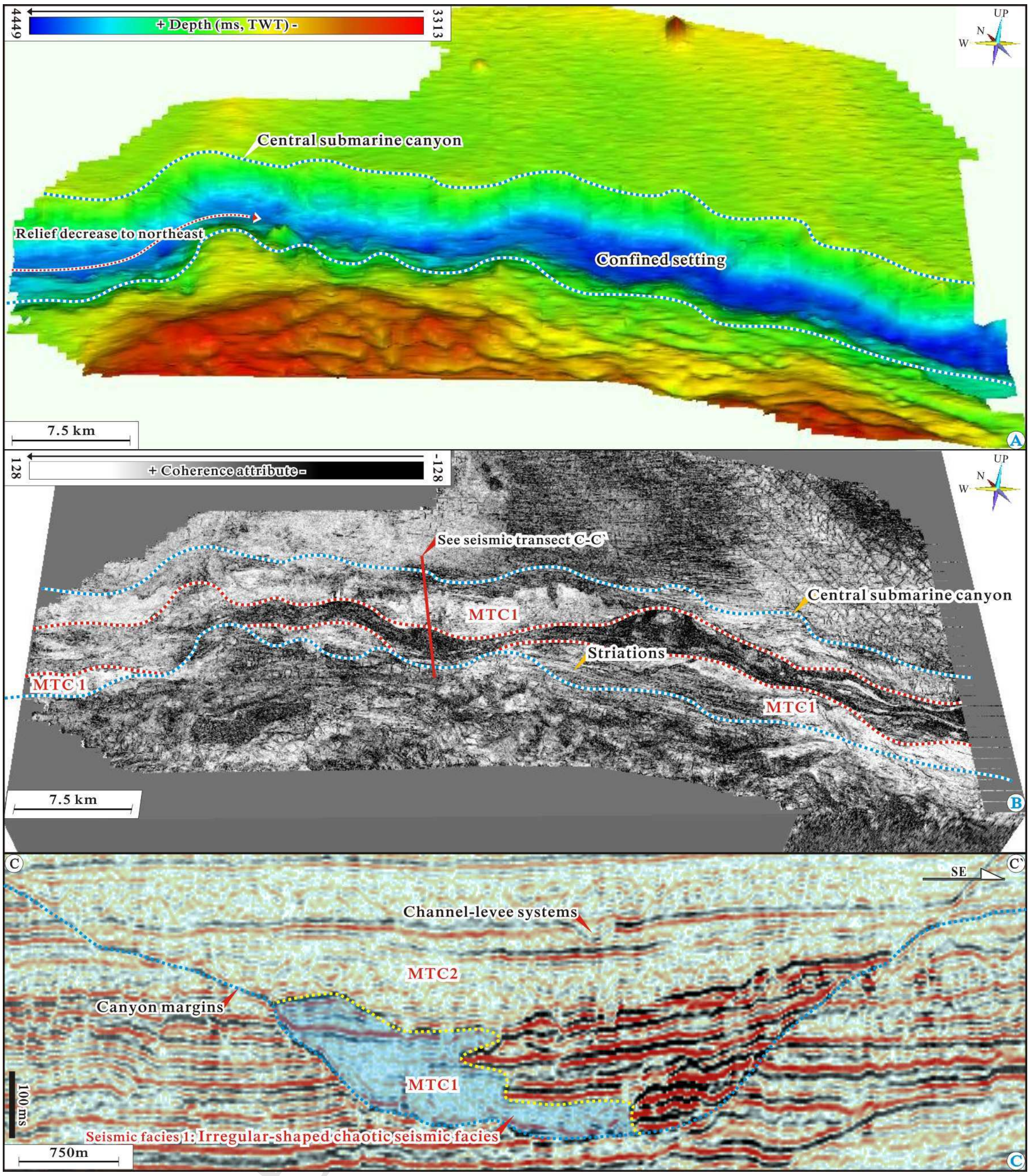

Figure 4. (Panel A) Three-dimensional perspective views of the basal bounding surface of MTC1 (BS1). Hot and cool colors on time-structure (ms TWT is millisecond two-way traveltime) maps presented in Figs. 4A to 11A represent topographic highs and lows, respectively. (Panel B) Coherence map of a slice 160 ms above the basal bounding surface of MTC1 (BS1) showing plan-view details of MTC1. Low and high coherence in plan-view geomorphic images derived from 3D coherence volumes presented in Figs. 4B to 11B are in dark and light colors, respectively. (Panel C) Cross-section looking downstream (for line location see Fig. 4B) illustrating seismic examples of detached MTCs seen as irregular-shaped chaotic seismic facies.

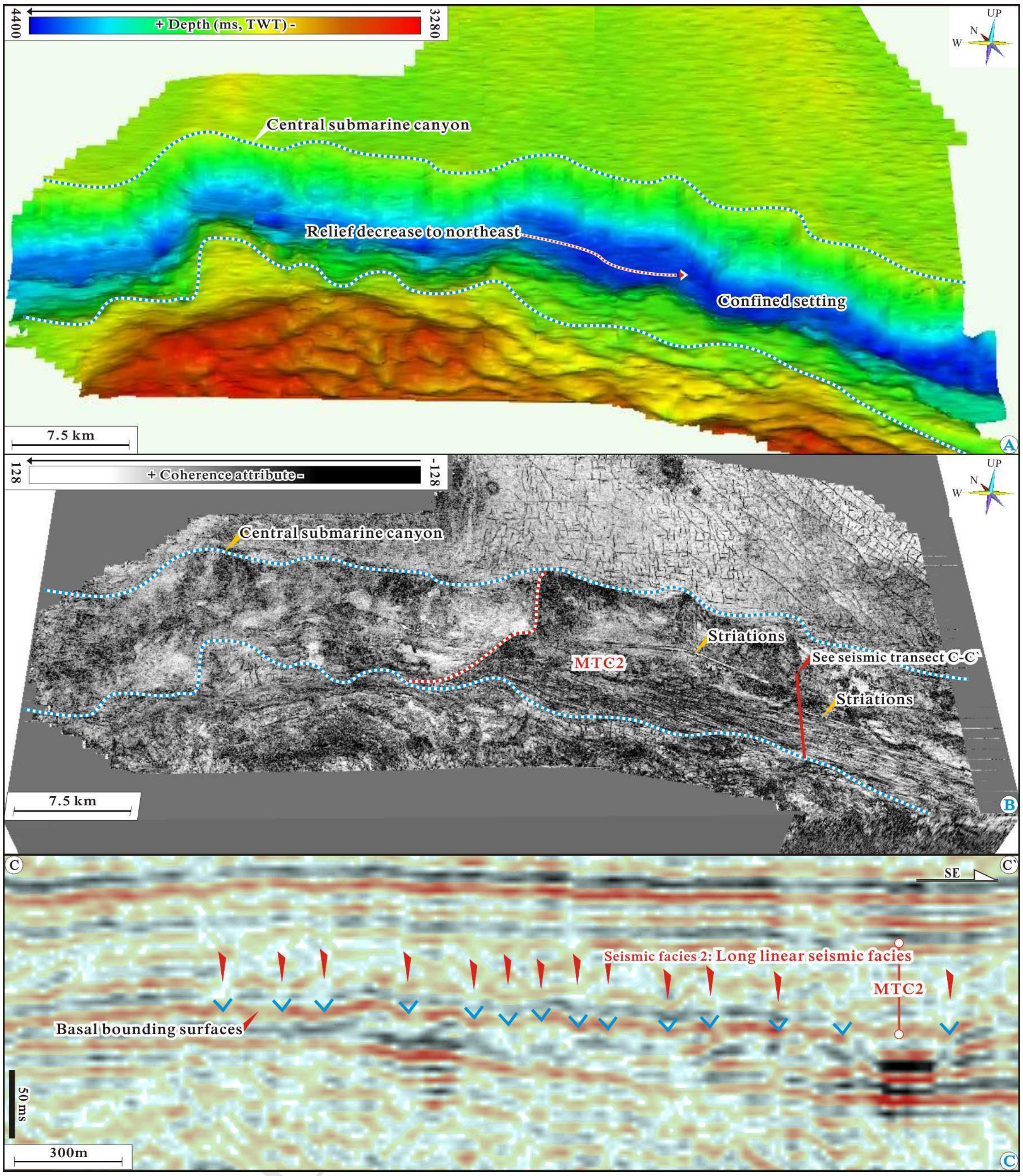

Figure 5. (Panel A) Time-structure map of basal bounding surface of MTC2 (BS2) showing a well-developed, slope-parallel topographic low for the development of MTC2. (Panel B) Flattened horizontal coherence slice at 155 ms above the basal bounding surface of MTC2 (BS2) illustrating plan-view details of MTC2 and its associated linear grooves. (Panel C) Cross-section looking downstream (see Fig. 5B for line location) showing seismic appearance of grooves seen as long linear seismic facies.

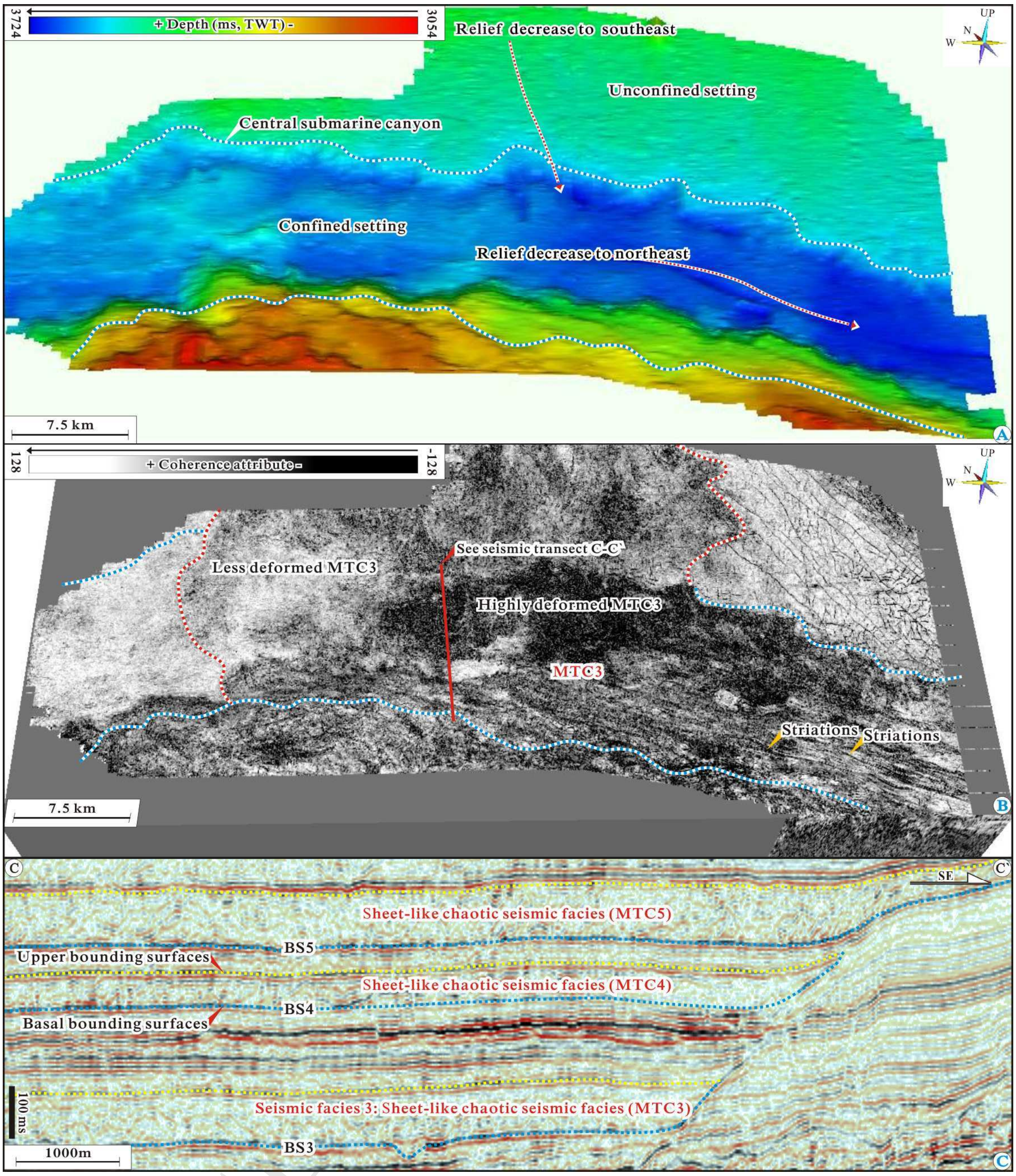

Figure 6. (Panel A) Three-dimensional perspective views of the basal bounding surface of MTC3 (BS3) showing a semi-confined, topographic low with a topographic relief increasing northeastward, within which MTC3 developed. (Panel B) Coherence image of a slice 100 ms above the basal surface of MTC3 (BS3) showing geomorphological expression of MTC3 and its associated grooves, less deformed MTCs and highly deformed MTCs. (Panel C) Strike-oriented seismic lines (location shown in Fig. 6B) showing seismic examples of attached MTCs seen as sheet-like chaotic seismic faceis.

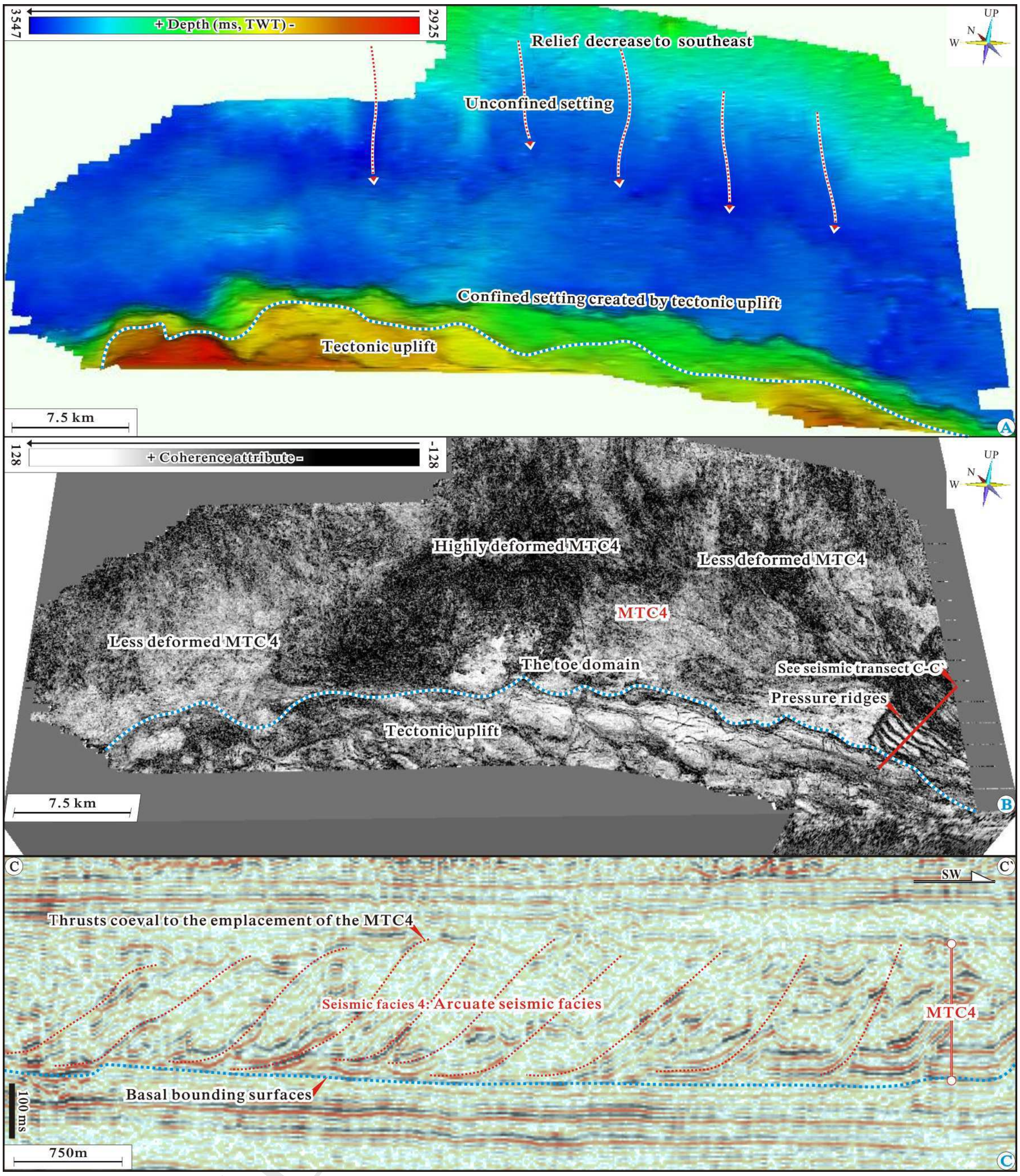

Figure 7. Shelf-attached MTCs (MTC4) recognized in the study area of Qiongdongnan Basin, as it appears on three-dimensional perspective view map of the basal bounding surface of MTC4 (BS4) and on the coherence slice taken 120 ms above the basal bounding surface of MTC4 (BS4) (upper and middle panels, respectively). (Panel C) Vertical seismic sections (line location shown in Fig. 7B) through the toe domain of MTC4 illustrating best-developed examples of landward inclined arcuate seismic facies interpreted as pressure ridges.

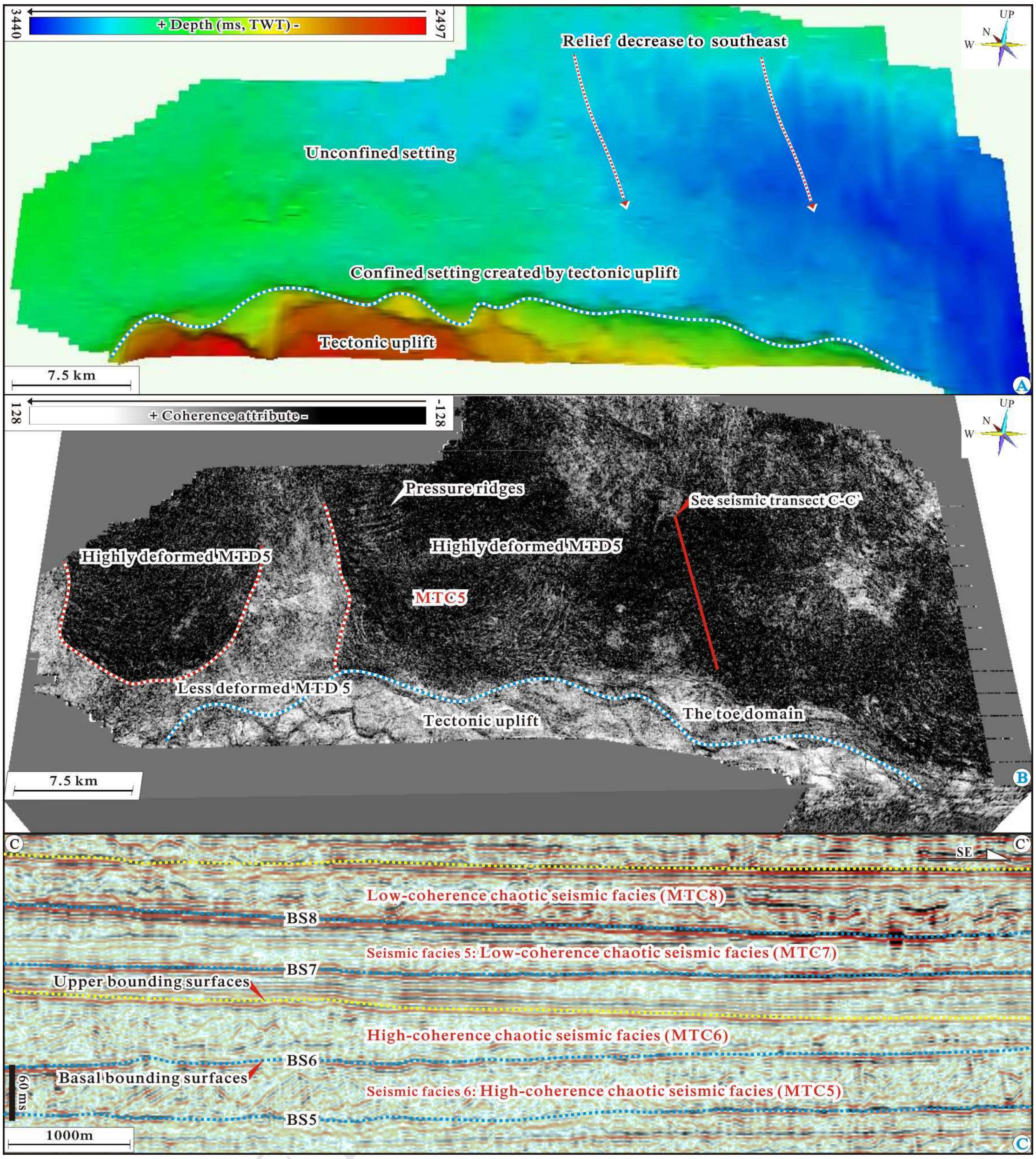

Figure 8. (Panel A) Time-structure map of the basal bounding surface of MTC5 (BS5) showing a semi-confined setting for the development of MTC5. Notice the southwestward decreasing in bathymetric relief and confinement. (Panel B) Flattened horizontal coherence slice seen at 120 ms above the basal bounding surface of MTC5 (BS5) illustrating seismic appearance of MTC5 and its associated highly deformed MTCs and pressure ridges. (Panel C) Strike-view cross section (see Figs. 8B and 11B for line location) to illustrate details of less and highly deformed MTCs seen as high- and low-coherence chaotic seismic facies, respectively.

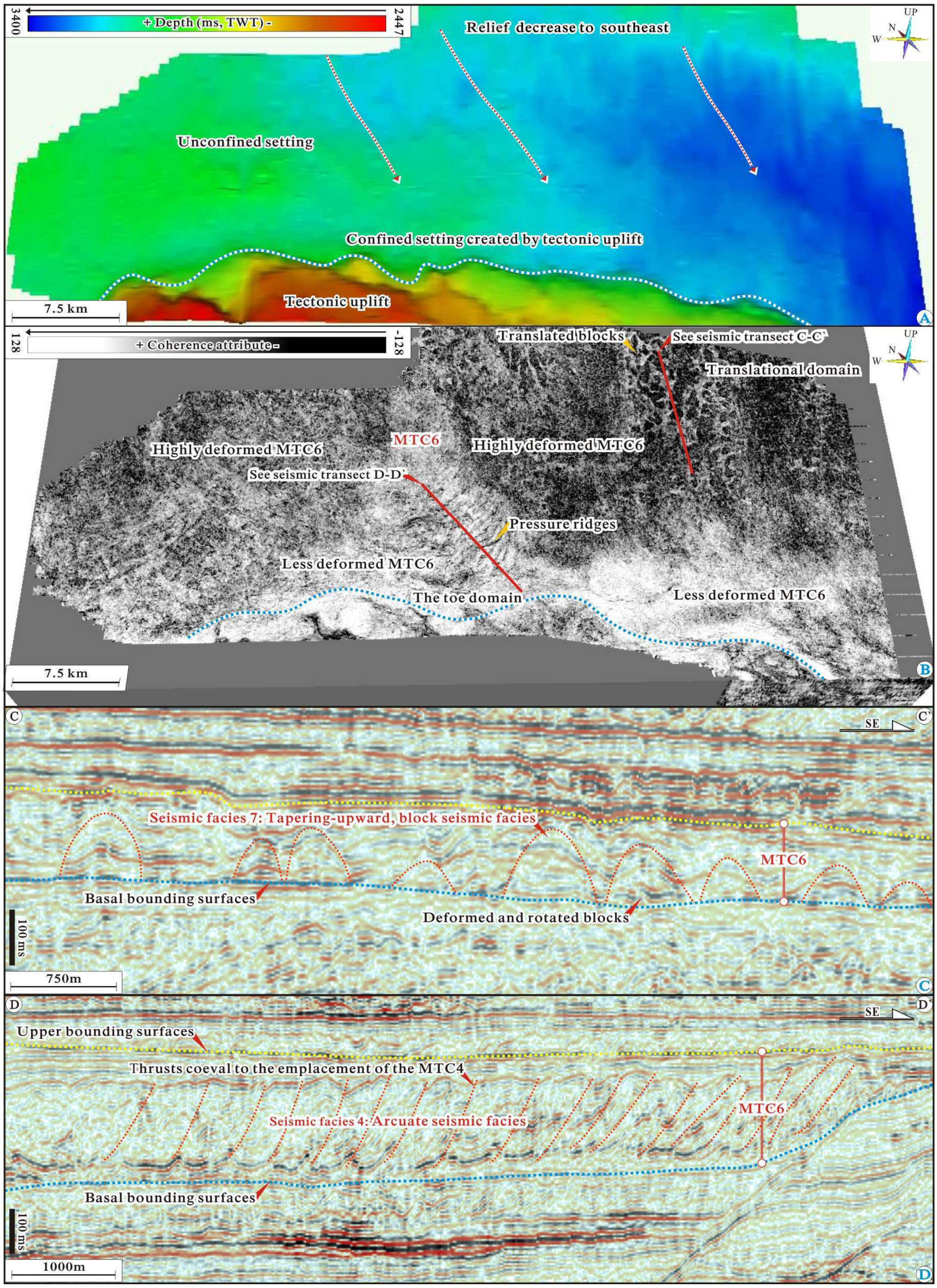

Figure 9. (Panel A) Three-dimensional perspective views of the basal bounding surface of MTC6 (BS6) illustrating a semi-confined setting for the development of MTC6. (Panel B) Flattered horizontal coherence image of a slice 120 ms above the basal bounding surface of MTC6 (BS6) showing plan-view geomorphological expression of MTC6. Seismic traverses (location shown in Fig. 9B) showing seismic appearance of translated blocks and pressure ridges (panels C and D,

respectively).

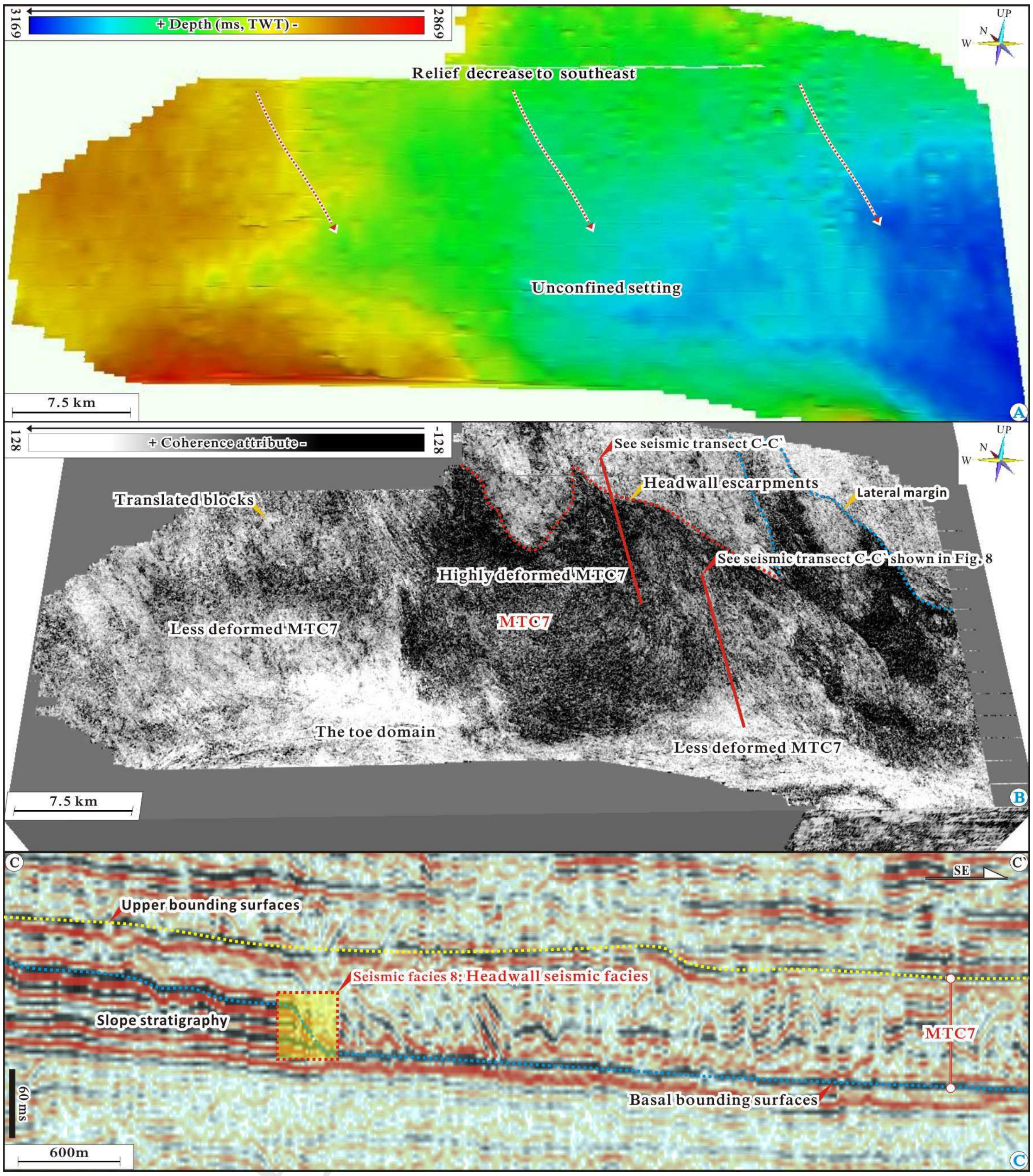

Figure 10. (Panel A) Time-structure map of the basal bounding surface of MTC7 (BS7) showing an unconfined setting for the development of MTC7. (Panel B) Flattened horizontal coherence slice at 150 ms above the basal bounding surface of MTC7 (BS7) illustrating the geomorphological expression of MTC7 and its associated grooves and headwall scarps. (Panel C) Zoomed in area of seismic section (location presented in Fig. 10B) through the headwall domain of MTC7 illustrating excellent seismic examples of basinward inclined arcuate seismic facies interpreted as MTC headwalls.

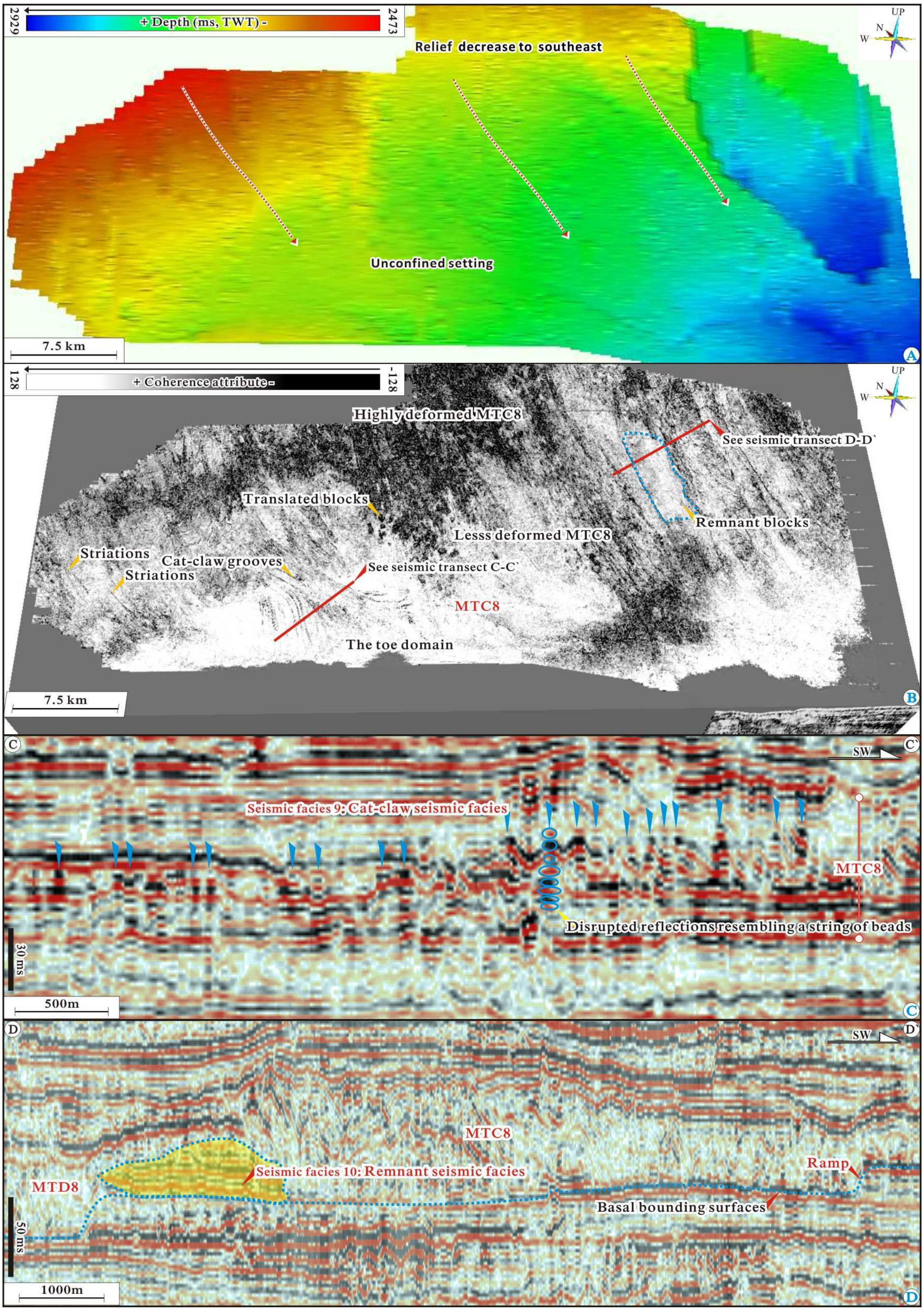

Figure 11. Shelf-attached MTCs (MTC8) appeared on three-dimensional perspective view of the basal bounding surface of MTC8 and on coherence slices taken 130 ms above the basal bounding surface of MTC8 (BS8) (upper and lower panels, respectively). Seismic sections (line location shown in Fig. 11B) showing seismic examples of cat-claw grooves and remnant blocks (panels C

and D, respectively).

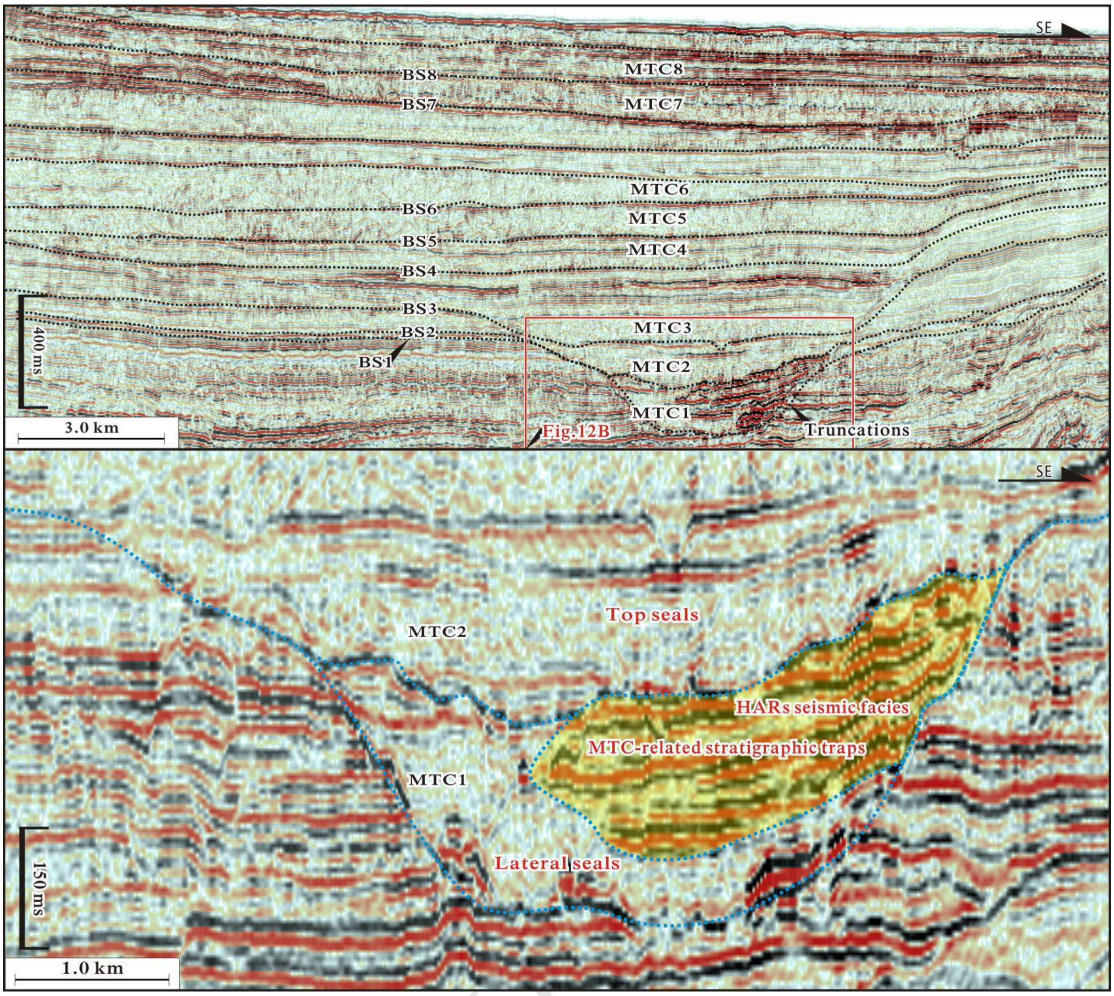

Figure 12. Dip-oriented seismic section (see Figs. 13 and 14 for line location) showing cross-sectional expression of potential MTC-related stratigraphic trap configuration (see hot color-shaded areas in the section) and channel fills (hot color-shaded area, HARs seismic facies). BS = Basal bounding surfaces. Please refer to Figure 13 for the plan-view seismic expression of MTC-related stratigraphic traps and channel fills and to text for a detailed discussion.

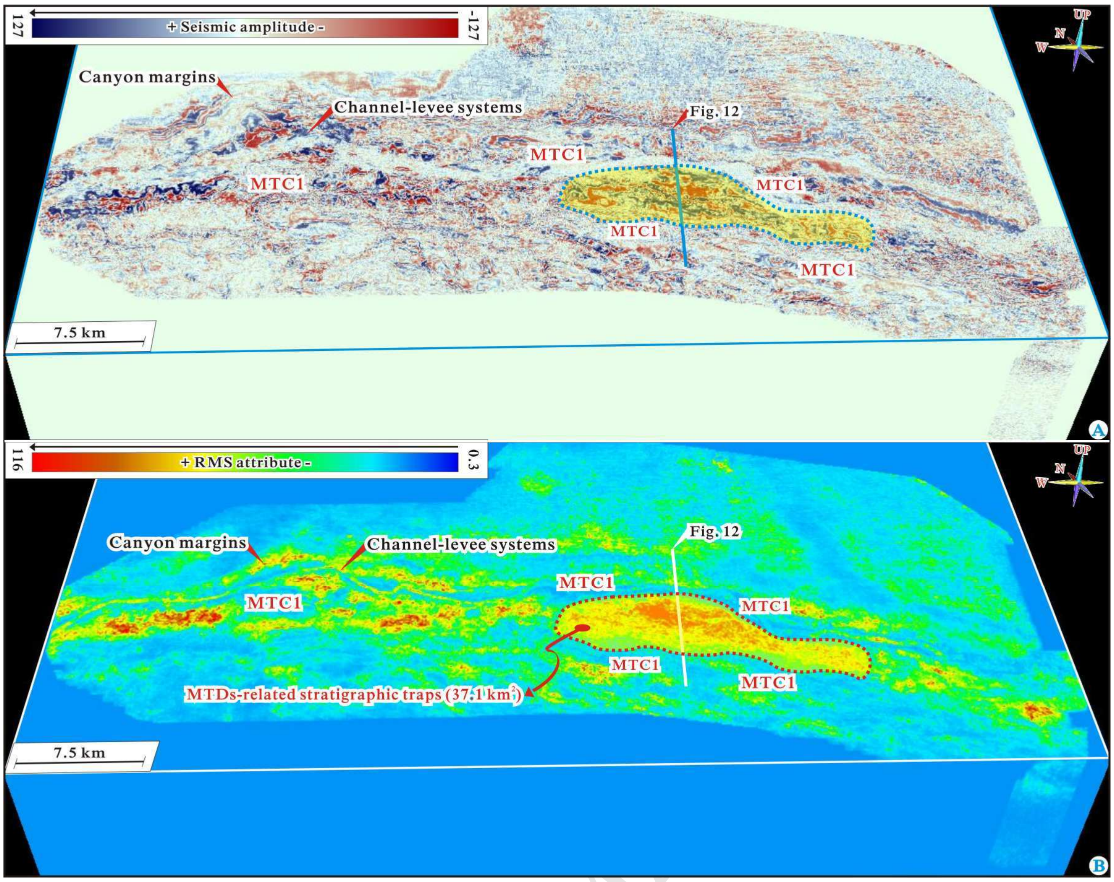

Figure 13. Channel fills seen as high-amplitude (panel A) and high-RMS-attribute zones (panel B) are blanketed and surrounded by detached MTCs, forming potential MTC-related stratigraphic traps (hot color-shaded areas) that are seen on plan-view geomorphic images derived from 3D amplitude and RMS attribute volumes (upper and lower images, respectively). Refer to Figure 12 for their cross-sectional details and to text for a detailed discussion.

- Eight MTCs were recognized and are classified as attached and detached MTCs.
- Detached MTCs were triggered by local instabilities.
- Attached MTCs resulted from large-scale collapses.
- MTC-related stratigraphic traps were identified.